EARTH SURFACE PROCESSES AND LANDFORMS
Earth Surf. Process. Landforms (2019)

Published online in Wiley Online Library
(wileyonlinelibrary.com) DOI: 10.1002/esp.4569

The mixed-bed glacial landform imprint of the North Sea Lobe in the western North Sea

David H. Roberts,[1]* Elena Grimoldi,[1] Louise Callard,[1] David J.A. Evans,[1] Chris D. Clark,[2] Heather A. Stewart,[3] Dayton Dove,[3] Margot Saher,[4] Colm Ó Cofaigh,[1] Richard C. Chiverrell,[5] Mark D. Bateman,[2] Steven G. Moreton,[6] Tom Bradwell,[7] Derek Fabel[8] and Alicia Medialdea[9]

[1] Department of Geography, Durham University, Durham, DH1 3LE, UK
[2] Department of Geography, University of Sheffield, Sheffield, S10 2TN, UK
[3] British Geological Survey, Lyell Centre, Research Avenue South, Edinburgh, EH14 4AP, UK
[4] School of Ocean Sciences, Bangor University, Menai Bridge, LL59 5AB, UK
[5] Department of Geography, University of Liverpool, Liverpool, L69 7ZT, UK
[6] Natural Environment Research Council, Radiocarbon facility, East Kilbride, Scotland, G75 OQF, UK
[7] Biological and Environmental Sciences, University of Stirling, Stirling, Scotland, FK9 4LA, UK
[8] SUERC, Rankine Avenue, Scottish Enterprise Technology Park, East Kilbride, G75 0QF, UK
[9] Geography Insitute, University of Cologne, Otto-Fischer-Str. 4 50674 Cologne, Germany

Received 11 May 2018; Revised 28 November 2018; Accepted 6 December 2018

*Correspondence to: D. H. Roberts, Department of Geography, Durham University, Durham, DH1 3LE, UK. E-mail: d.h.roberts@durham.ac.uk

ESPL
Earth Surface Processes and Landforms

ABSTRACT: During the last glacial cycle an intriguing feature of the British-Irish Ice Sheet was the North Sea Lobe (NSL); fed from the Firth of Forth and which flowed south and parallel to the English east coast. The controls on the formation and behaviour of the NSL have long been debated, but in the southern North Sea recent work suggests the NSL formed a dynamic, oscillating terrestrial margin operating over a deforming bed. Further north, however, little is known of the behaviour of the NSL or under what conditions it operated. This paper analyses new acoustic, sedimentary and geomorphic data in order to evaluate the glacial landsystem imprint and deglacial history of the NSL offshore from NE England.

Subglacial tills (AF2/3) form a discontinuous mosaic interspersed with bedrock outcrops across the seafloor, with the partial excavation and advection of subglacial sediment during both advance and retreat producing mega-scale glacial lineations and grounding zone wedges. The resultant 'mixed-bed' glacial landsystem is the product of a dynamic switch from a terrestrial piedmont-lobe margin with a net surplus of sediment to a partially erosive, quasi-stable, marine-terminating, ice stream lobe as the NSL withdrew northwards.

Glaciomarine sediments (AF4) drape the underlying subglacial mixed-bed imprint and point to a switch to tidewater conditions between 19.9 and 16.5 ka cal BP as the North Sea became inundated. The dominant controls on NSL recession during this period were changing ice flux through the Firth of Forth ice stream onset zone and water depths at the grounding line; the development of the mixed-bed landsystem being a response to grounding line instability. © 2018 John Wiley & Sons, Ltd.

KEYWORDS: British-Irish Ice Sheet; North Sea Lobe; ice stream onset; mixed-bed glacial landform assemblage

Introduction

During the last glacial cycle, the North Sea Basin (NSB) was overrun at various times both by the British-Irish Ice Sheet (BIIS) and the Fennoscandian Ice Sheet (FIS). As such it was an area characterised by complex ice sheet dynamics resulting from ice sheet coalescence, decoupling, ice divide migration, marine inundation and the switching on and off of ice streams (Graham *et al.*, 2007, 2011; Sejrup *et al.*, 2016; Patton *et al.*, 2017). A particularly intriguing glaciological attribute of ice sheet inundation of the NSB was the formation of the North Sea Lobe (NSL), nourished by ice emanating from Northern England and Scotland, flowing south and parallel to the English east coast and periodically surging (Boulton *et al.*, 1977; Eyles *et al.*, 1994; Boston *et al.*, 2010) (Figure 1). The vast majority of the evidence for the NSL has been derived from onshore glaciogenic sediment exposures, ice marginal geomorphology and palaeo-ice dammed lakes (Wood and Rome, 1868; Lamplugh, 1879, Bisat, 1932; Eyles *et al.*, 1982; Evans *et al.*, 1995; Catt, 2007; Bateman *et al.*, 2008, 2011, 2015, 2017; Evans and Thomson, 2010; Davies *et al.*, 2009, 2012a; Roberts *et al.*, 2013), however, few studies (with the exception of Davies *et al.*, 2011; Dove *et al.*, 2017) have focused on the offshore imprint of the NSL.

The flow trajectory of the NSL offshore has been correlated with the offshore subglacial footprint of the Wee Bankie and Bolders Bank Formations (Boulton *et al.*, 1985; Balson and Jeffrey, 1991; Cameron *et al.*, 1992; Gatliff *et al.*, 1994; Carr *et al.*, 2006; Davies *et al.*, 2011) (Figure 1), both thought to have been deposited during the last glacial cycle and often associated with the Dimlington Stade and the later onshore

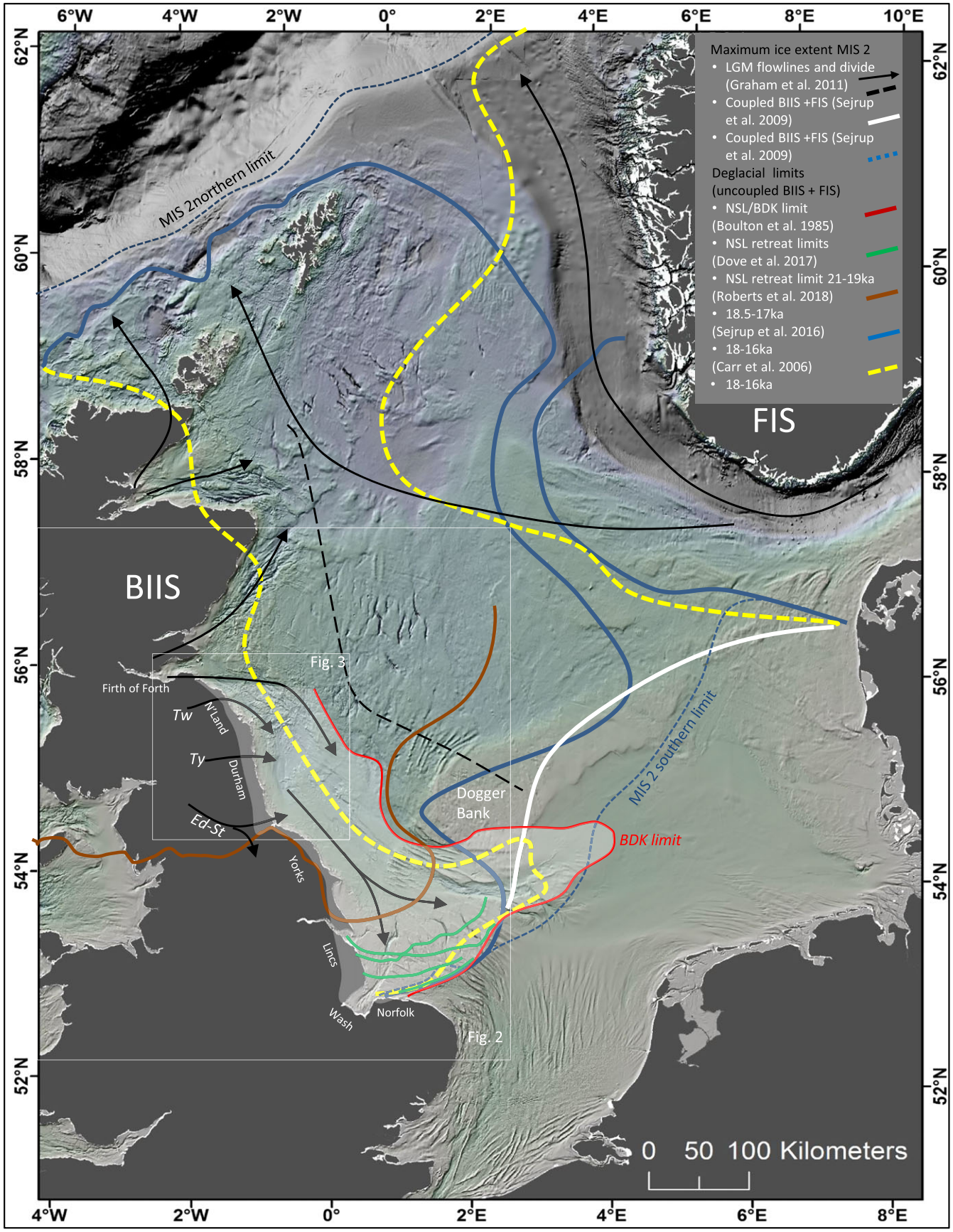

Figure 1. Bathymetric overview of the North Sea showing the position of BIIS and FIS ice margins, flowlines and ice divides during MIS 2 glaciation. The NSL was a distinctive lobe of ice that flowed southeast from the Firth of Forth region towards Norfolk in eastern England towards the end of MIS 2 glaciation. Its seafloor imprint has often been correlated to the distribution of Bolders Bank Formation (BDK) sediment, but controls on its hypsometry, dynamic behaviour and recession are poorly constrained. Major drainage basins feeding the NSL include the Firth of Forth, Tweed (Tw), Tyne Gap (Ty) and the Eden-Stainmore (Ed-St) gap (image based on reconstruction of Dove *et al.*, 2017 and Roberts *et al.*, 2018). [Colour figure can be viewed at wileyonlinelibrary.com]

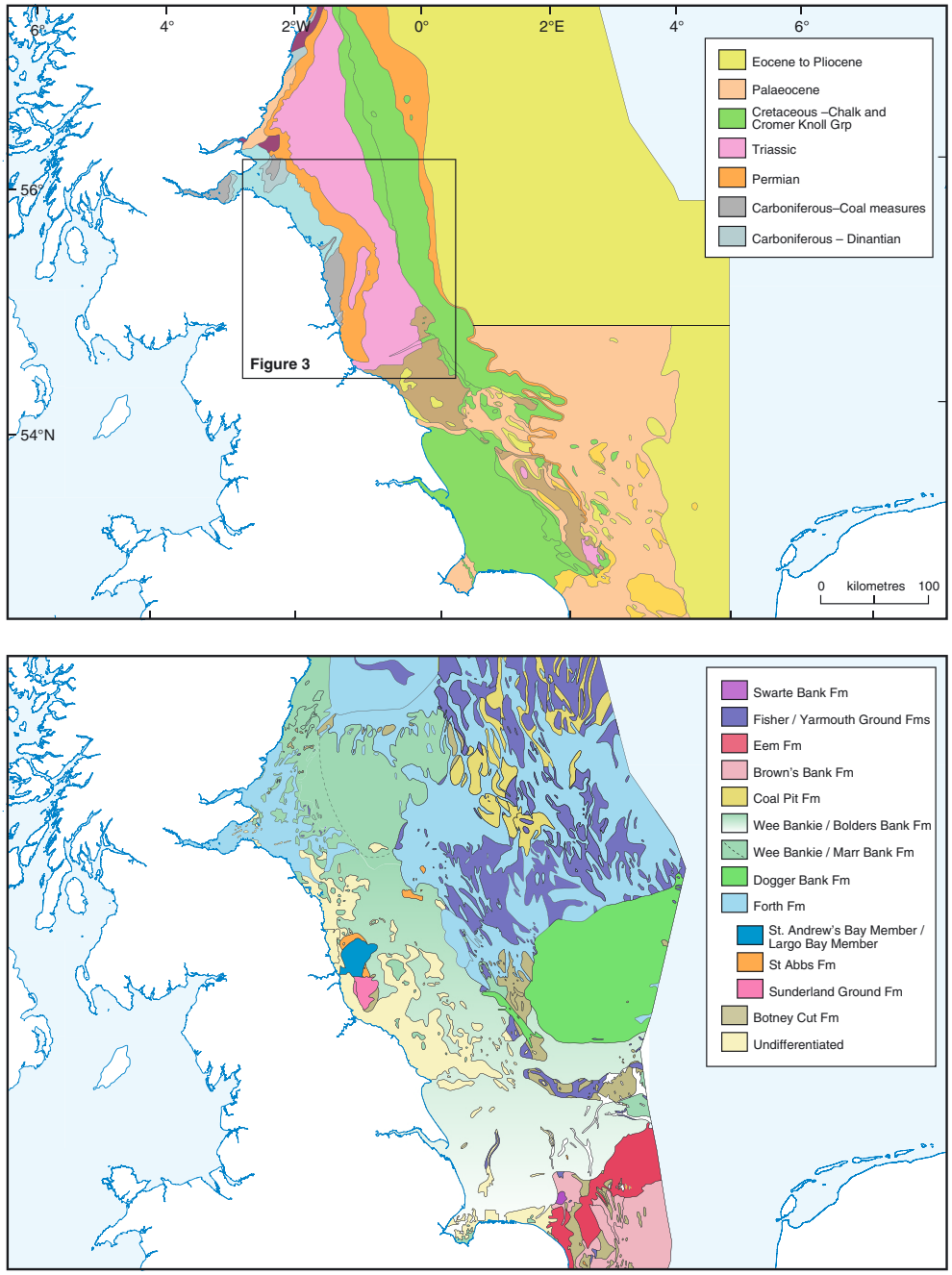

Figure 2. (a) Bedrock geology of the floor of the central western North Sea. Close to the Durham coast Carboniferous, Permian and Triassic rocks are prevalent. (b) The drift geology of the central western North Sea. Note the distribution of the Wee Bankie and Bolders Bank Formations which delimit the footprint of the North Sea Lobe. [Colour figure can be viewed at wileyonlinelibrary.com]

deposition of the Skipsea and Withernsea tills (Bateman *et al.*, 2011, 2017). Recently, Dove *et al.* (2017) have demonstrated that multiple tills associated with the Bolders Bank Formation form distinctive off-lapping sheets or arcuate moraines across the seafloor. They mark the northwards recession of the NSL from the Norfolk coast back towards North Yorkshire after 22.8 – 21.5 ka (Roberts *et al.*, 2018).

The stratigraphic architecture of the till sheets and moraines suggest a dynamic, oscillating margin operating over a deforming bed, with tunnel valleys indicating a surplus of meltwater during deglaciation (Dove *et al.*, 2017). Further north, however, in the area offshore from Durham and Northumberland, very little is known of the glaciogenic imprint of the NSL across the seafloor. The Wee Bankie Formation has been interpreted as a subglacial till, and the St Abbs, Forth, and Sunderland Ground formations as deglacial phase glaciomarine sediment (Cameron *et al.*, 1992; Gatliff *et al.*, 1994) (Figure 2), but the geomorphic imprint of the NSL and its recessional history have not been adequately constrained. Given the NSL was sourced from central Scotland via the Firth of Forth, the influence of the NSL on the BIIS in terms of ice divide migration, ice drawdown and flow trajectory would have been significant (particularly during deglaciation; Roberts *et al.*, 2018). Yet it remains unclear as to whether the NSL behaved as an ice stream, a terrestrial piedmont lobe or a tidewater terminating glacier (Golledge and Stoker, 2006; Boston *et al.*, 2010; Dove *et al.*, 2017). Thus a better understanding of the NSL's duration, style and retreat pattern is important not only to reconstruct BIIS dynamics but also with respect to the development of robust ice sheet models.

This paper analyses acoustic, sedimentary and geomorphic data collected by the BRITICE-CHRONO project and collated under the Glaciated North Atlantic margins (GLANAM) project in order to evaluate the glacial landsystem imprint of the NSL offshore from Durham and Northumberland. Furthermore, it

assesses evidence for a subglacial to glaciomarine transition during deglaciation, and establishes the timing of deglaciation offshore as ice moved back towards the Firth of Forth.

Regional Setting

The study area is situated offshore of the Durham and Northumberland coasts, and runs from Eyemouth in the north to Sunderland in the south (Figures 1, 2). It covers around 25 000 km^2 of the seabed. The region is underlain by Carboniferous, Permian and Triassic rocks (Figure 2(a)) (Cameron *et al.*, 1992), above which several Quaternary glaciogenic formations have been mapped. Immediately offshore, the Quaternary sediments are thin, with bedrock commonly exposed at the seabed. Beyond 15 km offshore the Quaternary sediments begin to thicken eastward. With respect to the last glacial cycle they include the Wee Bankie Formation, which is interpreted as subglacial in origin and probably contiguous with Bolders Bank Formation further south (Figure 2(b); Stoker and Bent, 1985; Gatliff *et al.*, 1994). It is composed of stiff diamicton with interbeds of sand, pebbly sand and silty clay (Cameron *et al.*, 1992; Gatliff *et al.*, 1994; Davies *et al.*, 2011). The Forth Formation is variously described as a series of marine, glaciomarine, fluviomarine and estuarine sediments. It occurs in pockets across the seafloor (Cameron *et al.*, 1992; Gatliff *et al.*, 1994). The St Andrews Bay and Largo Bay Members are related to the Forth Fm, and the St Abbs and Sunderland Ground Formations also probably represent deglacial glaciomarine conditions with transitions to upper Holocene marine sediments (Figure 2(b)). An alternative explanation for the Sunderland Ground Fm is deposition in a glaciolacustrine environment as an extension of glacial lake Wear (Catt, 2007).

Glacial sediments deposited by the NSL can also be found along the Northumberland and Durham coasts. The lower diamicton of the Warren House Formation is an MIS 8 to 12 glaciomarine deposit and was renamed the 'Ash Gill Member' (Davies *et al.*, 2012b). The Blackhall and Horden Till Formations and the Peterlee Sand and Gravel Formation along the Durham coast date to MIS 2 (Davies *et al.*, 2009, 2012a). The Blackhall Till Formation originated in north-western England and was deposited by the Tyne Gap Ice Stream (Davies *et al.*, 2009), but the Horden Till was deposited by the NSL with ice originating from Scotland and moving south via the Cheviots and Northumberland coast (Everest *et al.*, 2005; Davies *et al.*, 2009; Livingstone *et al.*, 2012). Glaciolacustrine sediments associated with glacial lakes Wear and Tees also crop out at the coast and may be contiguous with the Sunderland Ground Formation offshore. The ice marginal geomorphic imprint of the NSL pushing onshore can be discerned in a series of linear kames, moraines, eskers and ice dammed lake basins that run north to south from Berwick-upon-Tweed to the Tees (Teasdale, 2013; Livingstone *et al.*, 2015).

The imprint of the NSL offshore with respect to both ice advance and retreat is poorly constrained. The footprint of the Wee Bankie Formation may be contiguous with the Bolders Bank Formation further south, and if so, the Wee Bankie Formation sediments may mark the passage of the NSL during both advance and recession along the north coast of England during the last glacial cycle (Balson and Jeffrey, 1991; Carr *et al.*, 2006). It is most likely that the NSL was fed by ice from Scotland through the Firth of Forth which may have acted as an ice stream onset zone (Boulton and Hagdorn, 2006; Golledge and Stoker, 2006; Hubbard *et al.*, 2009), though in the southern NSB the geomorphic imprint of the NSL and the association of subglacial and glaciofluvial sediments points to a terrestrial piedmont lobe (Dove *et al.*, 2017). During deglaciation, optically stimulated luminescence samples (OSL) from Norfolk show the ice first receded northwards after 21.5 ka (Roberts *et al.*, 2018) and that ice departed the Yorkshire coast as late as ~ 17.6 ka (Bateman *et al.*, 2017; Evans *et al.*, 2017). Livingstone et al. (2015) propose deglaciation of the area west of Newcastle at 17.8 to 17.6 ka based on Be^{10} exposure ages. Finally, there are multiple dates around the edges of the Firth of Tay and Firth of Forth which suggest ice had retreated into that part of Scotland by 17.0–16.5 cal. ka BP with glaciomarine environments on-lapping the present coast (Hedges *et al.*, 1989; Peacock and Browne, 1998; Peacock, 2002). These ages suggest a window of recession of ~1000 yrs for the NSL between Yorkshire and the Firth of Forth towards the end of the Last Glacial Maximum (LGM) (Figure 1).

Methods

The bathymetric data included in this paper where downloaded from the UK Hydrographic Office (UKHO) under the Open Government Licence v3 and cover an area which extends up to ~125 km from the coastline, from Eyemouth in the north to Sunderland in the south (Figure 3(a)). A Digital Elevation Model (DEM) of the UKHO data was created at 50 m horizontal resolution. An area of multibeam bathymetry data located approximately 11 km off the Northumberland coast, covering an area of approximately 705 km^2 was provided courtesy of Defra. A DEM of the Defra data was created at 5 m resolution. The GEBCO 2014 grid and Olex database for the North Sea (www.olex.no) were also used to provide regional bathymetric information for the western North Sea. The combined bathymetric surfaces were used for geomorphological interpretation.

The shallow sub-seabed geology was interpreted from a mixture of sub-bottom profiler (chirp) data collected during cruise JC123 onboard the RRS James Cook in August 2015, and digital scans of single-channel seismic (surface tow boomer and sparker) data acquired by the British Geological Survey from the 1970s to 1990s (Fannin, 1989). Chirp data was collected using a hull mounted Kongsberg SBP-120 sub-bottom profiler that operated a sweep frequency between 2500 and 6500 kHz with a depth resolution of 0.3 ms. All seismic data were interpreted using the IHS Kingdom™ software.

Seven vibrocores are described in detail. They were retrieved using the British Geological Society vibrocorer with a 6 m barrel and 8 cm core diameter. The cores were measured for magnetic susceptibility (MS) and gamma density, using Geotek Multi-Sensor Core Logger (MSCL) at two centimeter resolution (see Supplementary information). A Geotek XCT scanner provide X-radiographs. Shear vane measurements using a hand held Torvane was carried out on-board. Sedimentary facies are described following Evans and Benn (2004). These cores are supplemented by unpublished data from core 118VC from the area west of the Firth of Forth and a glacial sediment section from the coast at Seaham. Both sites provide additional onshore/offshore context relating to regional deglacial history.

Micropalaeontological analysis on foraminifera was attempted on all the cores. Each sample was wet sieved through 500 µm and 63 µm sieves. Foraminifera were dry picked from the 63 to 500 µm fractions under a Zeiss Stemi SV11 binocular microscope. Studies on benthic foraminifera species for paleoenvironmental reconstructions usually require a minimum of 300 individuals to obtain a reliable indicator of the species diversity (Jennings *et al.*, 2014). However, due to low species abundance only two sample counts were >200 with the majority of counts less than 100. The foraminifera assemblages instead provide an indication of the depositional palaeoenvironment.

A total of five radiocarbon samples, including one bivalve and four mixed benthic foraminifera samples, from four cores (118VC, 128VC, 132VC and 137VC), were submitted for

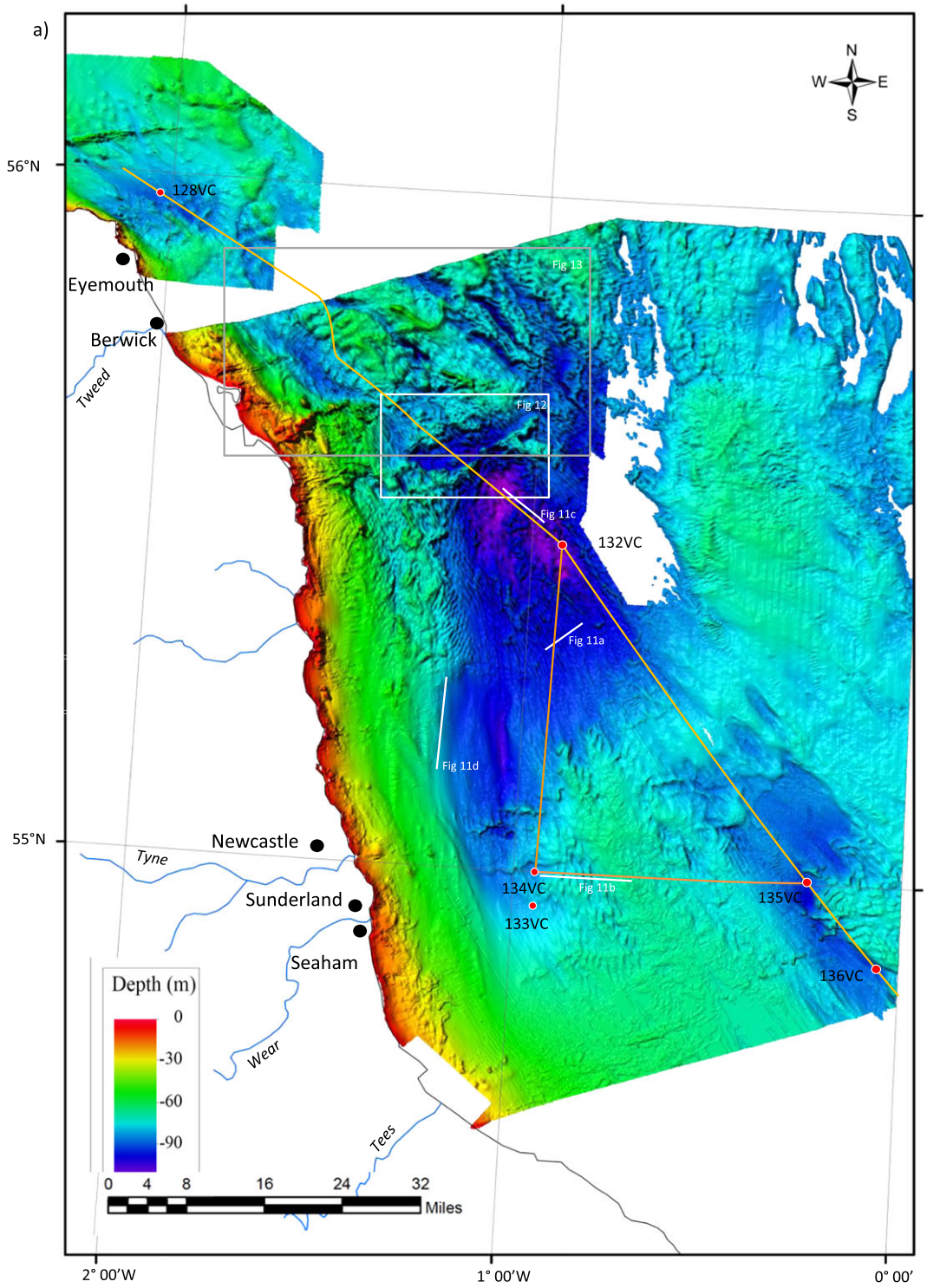

Figure 3. (a) Bathymetry of the central western North Sea close to the northeast coast of England. The areas immediately offshore between Seaham and Eyemouth are very shallow but deepen to 113 m in the central study area. (b) Several distinctive landforms can be mapped across the seafloor. They include sediment wedges and ridges, lineations, channels and bedrock ridges. [Colour figure can be viewed at wileyonlinelibrary.com]

analysis. The whole bivalve was cleaned with deionised water and dried at 40°C. The foraminifera samples were dry picked from the 500 and 63 μm fractions. The samples were submitted to the NERC radiocarbon facility in East Kilbride where they were hydrolysed to CO_2 using 85% orthophosphoric acid at room temperature and reduced to graphite using a two-stage reduction over heated Zn and Fe (Slota *et al.*, 1987). The prepared graphite targets were passed to the SUERC AMS laboratory or the Keck C Cycle AMS laboratory, University of California, Irvine for ^{14}C measurement. The conventional ages were calibrated using OxCal 4.2 calibration programme (Bronk Ramsey, 2009) with the Marine13 curve, an inbuilt marine reservoir correction of 400 years and a ΔR of 0 years (Reimer *et al.*, 2013). The ages are reported in the text as the calibrated 2σ median result (Table I). Only the calibrated ΔR of 0 are used in the text.

Three sand samples from glaciofluvial facies exposed on the coast at Seaham were collected in opaque PVC tubes for optically stimulated luminescence (OSL) dating (Table II). These were prepared following standard procedures to isolate and clean the quartz fraction (see Bateman and Catt, 1996). Dose

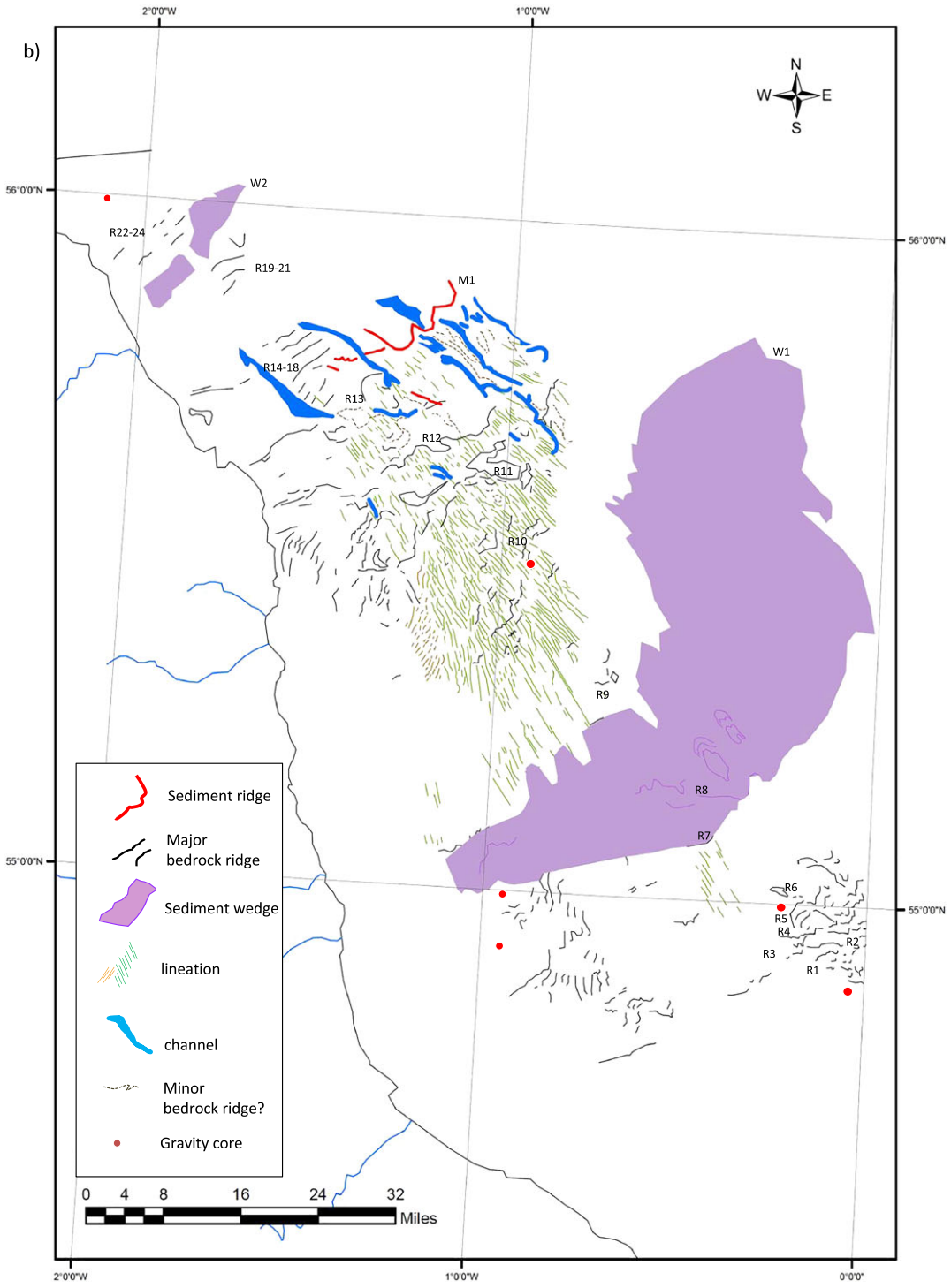

Figure 3. (continued)

rates were based on radionuclide concentration determined by inductively coupled plasma mass spectroscopy for the beta dose rate contribution and *in situ* gamma spectrometry for the gamma dose rate. A cosmic dose rate was calculated based on average burial depths through time using the algorithm of Prescott and Hutton (1994). Dose rates were appropriately attenuated for grain size and palaeomoisture. The latter were estimated at 23% to reflect the stratigraphic positions of the sand unit sampled in an aquiclude between two diamicts. OSL measurements used automated Risø readers with blue (470 nm) LEDs and were on ultra-small multigrain aliquots (SA, containing 20 grains each). All samples were measured using the SAR protocol (Murray and Wintle, 2003) including an IR depletion ratio step to test for feldspar contamination and a pre-heat of 220°C for 10 s. The latter was derived experimentally from a dose recovery preheat test. For each sample, 60-92 SA replicates were measured. Derived D_e estimates were accepted if the relative uncertainty on the natural test dose response was <20%, the recycling and the IR depletion ratio (including uncertainties) were within 20% of unity and recuperation <5%.

The resulting OSL data showed D_e distributions were non-normal and too highly scattered (over-dispersion ranged from 72 to 83%) to be considered as belonging to well bleached sediments. As a result the internal-external consistency model (IEU, Thomsen *et al.*, 2007) was adopted to derive an estimate the true (bleached) burial dose with the starting parameters based the results from the well bleached samples from Heslerton (see Evans *et al.*, 2017 for details). Such an approach

Table I. Radiocarbon ages from offshore cores 118VC, 128VC, 132VC and 137VC. Conventional radiocarbon ages and calibrated ages are shown without marine reservoir correction due to uncertainties over the temporal variation of the marine reservoir effect

Lab code	Sample core and depth	Geological context and material dated	$\delta^{13}C_{VPDB}$‰ (± 0.1)	Conventional radiocarbon age (years BP ± 2 σ)	Calibrated age +/- 2σ (Cal BP)
SUERC-68009	T2-128VC-280	Laminated glaciomarine seds; Mixed foraminifera assemblage	-1.146	14445 ± 112	16949 ± 216
SUERC-68010	T2-132VC-144	Laminated glaciomarine seds; Mixed foraminifera assemblage	-1.459	16708 ± 130	19571 ± 172
UCIAMS-176372	T2-137VC-552	Laminated glaciomarine seds; Mixed foraminifera assemblage	-1.237	16900 ± 120	19895 ± 218
SUERC-68001	T2-118VC- 240a	Laminated glaciomarine seds; Nuculana pernula	0.470	15157 ± 120	17862 ± 169
SUERC-68007	T2_118VC_240b	Laminated glaciomarine seds; Mixed foraminifera assemblage	-1.845	14206 ± 114	16529 ± 235

Table II. OSL age data for samples from glacial outwash sediments at Seaham, County Durham. These sit between the Blackhall and Horden Tills are therefore represent deposition along the western NSL ice margin just prior to final deglaciation. Data includes palaeomoisutre (w), total dose rate, number of aliquots measured and accepted in brackets, the derived estimated equivalent doses (D_e) and resultant ages

Lab code	Field code	W (%)	Beta dose rate (Gy/ka)	Gamma dose rate (Gy/ka)	Total dose rate (Gy/ka)	n	D_e (Gy)*	OD (%)	Age (ka)
Shfd14064	Sea14/1/1	23	539 ± 43	586 ± 31	1.14 ± 0.05	91 (47)	22.6 ± 1.8	72	19.8 ± 1.8
Shfd14065	Sea14/1/2	23	539 ± 41	569 ± 31	1.13 ± 0.05	92 (47)	21.7 ± 1.4	93	19.1 ± 1.9
Shfd14066	Sea14/1/3	23	465 ± 36	710 ± 40	1.12 ± 0.05	66 (35)	23.8 ± 2.5	83	19.9 ± 2.3

*D_e derived using IEU

has been shown to be appropriate to estimate accurate ages for incompletely bleached glacial sediments (Bateman *et al.*, 2017). Ages are reported in Table II calculated from the time of measurement (2013) with one sigma uncertainties.

Results

Regional bathymetry and seismic data

The area offshore from Durham and Northumberland is very shallow (Figure 3(a)). To the north, water depths do not exceed ~ –80 m. Further south, waters are up to 40 m deep along the coastline but deepen eastward and average ~ –70 m. However, local basins in the central part of the study area reach a maximum depth of –113 m. (Figure 3(a)). Where the seafloor is relatively smooth it is covered by soft sediment. In other areas, bedrock is close to, or at, the seafloor (Figure 3(a), (b)).

Five different acoustic facies were mapped across the study area (Figures 4 and 5). AF1 is the lowermost facies of the sequence and is composed mainly of Permian bedrock, though Triassic, Cretaceous and Jurassic rocks are present in the study area (Cameron *et al.*, 1992; Gatliff *et al.*, 1994) (Figures 2, 5(a), (b)). Bedrock is generally present at very shallow depths below the seabed, forming the distinctive topography of the seafloor. It is often heavily folded and faulted with strata orientated subvertically in many areas (Figure 5(a)). There are also several intrusive complexes forming ridges on the seafloor, with ridges R6 and R11 being particularly clear examples (Figure 4(a)). There are four acoustic facies that can be mapped above the bedrock (AF2–AF5). They have a patchy distribution across the study area, being laterally discontinuous and of variable thickness (Figures 4 and 5).

AF2 is laterally discontinuous and relatively thin, occurring only as isolated lenses of sediment (Figure 4). On average it is 2–6 m thick and lies directly on bedrock. It is internally transparent and structureless but its upper surface is often characterised by low amplitude, irregular bumps (e.g. Figure 5(a)). AF3 is the most ubiquitous facies in the study area and occurs over the bedrock or lenses of AF2. AF3 exhibits variable thickness, being thickest (10–25 m) where it forms the core of wedges W1 and W2 (Figure 4(a), (b)). Between W1 and W2 it thins in places to only 1–2 m, and often disappears over bedrock bedforms. In some locations (irrespective of the underlying bedrock) AF3 is characterised by an undulating upper surface (Figure 5(a)). Internally, the facies is often slightly more opaque than AF2 and structureless, with the exception of occasional chaotic reflectors.

AF4 overlies AF3, although it occasionally lies directly on top of bedrock strata. Its acoustic appearance is defined by high frequency, parallel sub-horizontal reflectors (Figure 5(a)). It often infills small depressions and basins (Figure 4), and hence thickens and thins across the study area. At its thickest it is typically 8–10 m, although in local basins in the south and west it deepens to 20–25 m. In Figure 5(a) the internal reflectors within AF4 are wavy and appear to mimic the underlying 'bumpy' surface of AF3. The upper boundary of AF4 is usually flat. AF5 is the uppermost facies of the seismic sequence. It is thin, laterally discontinuous and difficult to map where bedrock is close to the seafloor. It is acoustically transparent on seismic profiles (Figures 4, 5 and 6).

Sediment cores

Seven vibrocores from the study are described in detail (128VC, 132VC, 133VC, 134VC, 135VC, 136VC, 137VC).

Core 128VC is located to the north of our study area (Figures 3(a), 4(a)). It is 4.5 m long and captures both AF3 and AF4, which directly overlay Carboniferous (Dinantian) bedrock (Figures 6 and 7(a)). The basal 59 cm is a brown, matrix supported, diamict (Dmm; AF3) containing abundant sub-rounded to sub-angular clasts in a silty matrix. Shear strengths increase downwards from 18 kPa to 68 kPa. Magnetic suspectibility (MS) is also high and increases with depth (see Supplementary information). The lower Dmm is transitional upwards to a stratified diamict (Dms) between 400 and 360 cm, with sorted, planar horizontal, draped laminae becoming interspersed with diamictic material. The lower Dms is transitional to a 72 cm thick laminated silt and clay unit (Fl); Figure 7(a)), which in turn is overlain by 236 cm of soft (<10 kPa), colour banded clay that

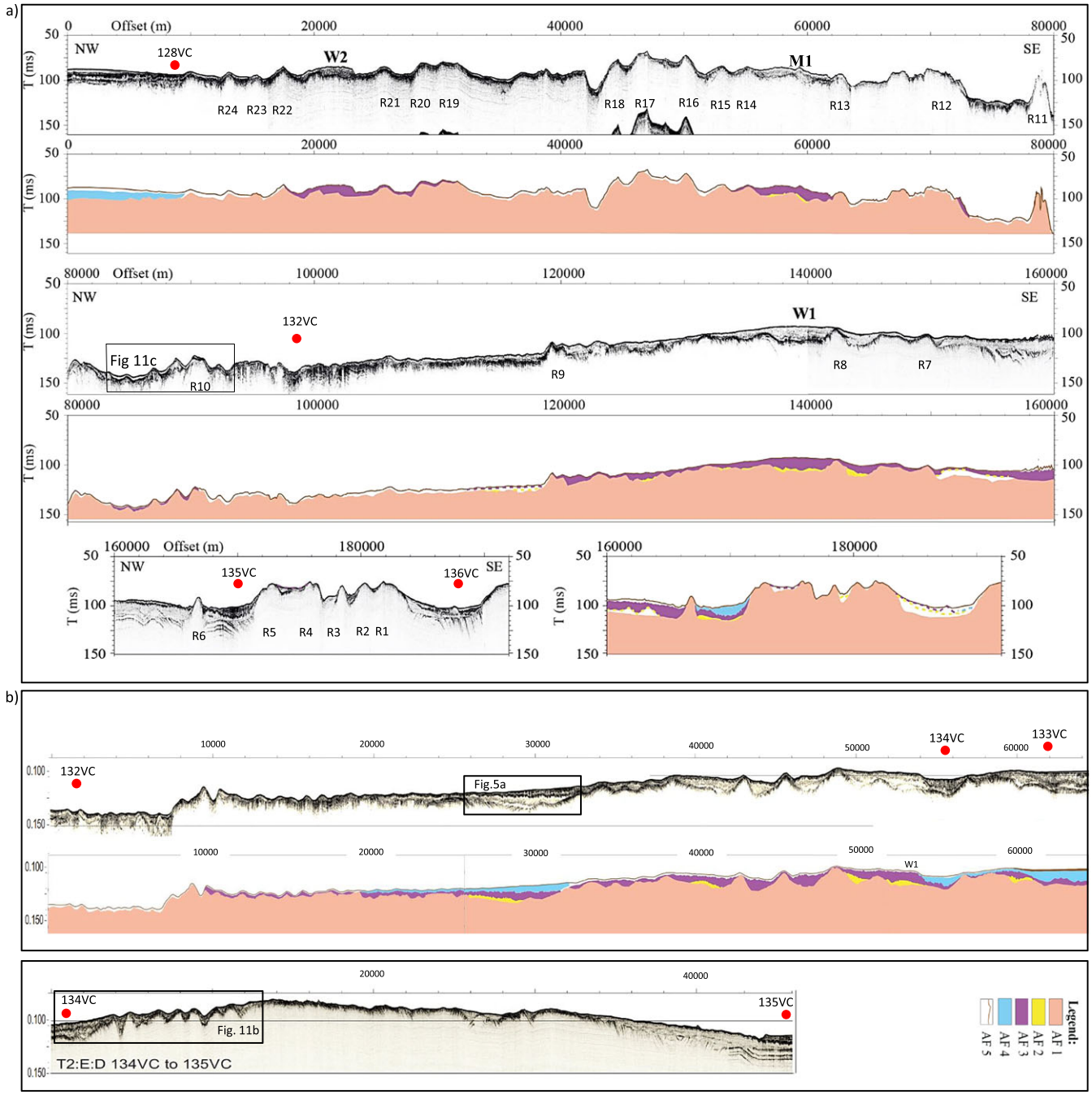

Figure 4. Sub-bottom profile data gathered from the study area. Note the position of several bedrock ridges (R1–24); sediment wedges W1 and W2 and ridge M1. Five distinctive acoustic facies can be mapped (AF1–5). AF1 is bedrock. AF2 and AF3 are diamictic, while AF4 is a stratified/laminated sediment package composed of fines. AF5 is a sandy facies with a distinctive reworked shell assemblage. (a) Acoustic data from the seafloor between core 128 VC and 136VC running NW to SE across the study area. (b) Acoustic data from the seafloor between core 132VC and 133VC and the area from 134VC to 135VC (see Figure 3(a) for location of cores). [Colour figure can be viewed at wileyonlinelibrary.com]

is occasionally laminated and contains thin sandy silt lenses (Fl/Sl; AF4). The core is capped by ~ 80 cm of shelly, silty sand with shell fragments increasing in abundance down core (AF5). One mixed benthic foraminifera sample from 280 cm down core in the (laminated silt and clay) provided a radiocarbon age of 16,949 ± 216 cal. BP (Table I). Samples for foraminifera analysis where taken at 20 cm resolution below 60 cm in the core. There were no foraminifera present in the Dmm and only low abundance in the Fl unit, with the species assemblage dominated by *Elphidium clavatum*.

Core 132VC is located approximately 20 km south-west of R11 (Figure 3(a), 4(a)) and was collected from a trough adjacent to a bedrock-cored lineation. Seismic data suggest the core sampled a lens of AF4 though it did not penetrate AF3 (Figure 6). Permian strata are present underneath the Quaternary sediments at this location. The base of core 132VC is characterised by 79 cm of very soft, laminated silty clay, which contains clear colour banding from red to brown, occasional 0.5–1 cm thick silt bands and outsize clasts (Figure 7(b); Fl(d)). The Fl(d) is overlain by 26 cm of dark grey/brown, soft, matrix supported Dmm that contains abundant clasts within a silty clay matrix. MS and gamma density are both high in the Dmm (see Supplementary information. The Dmm is overlain by a, soft, massive, brown clay (Fm) that contains the occasional silt/fine sand lenses. This Fm unit is truncated by a 16 cm layer of gravelly, silty, sand (Sm/Glag) with abundant shell valves and fragments. The top 54 cm of the core consists of dark brown, massive, silty sand (Sm), with occasional presence of shell fragments.

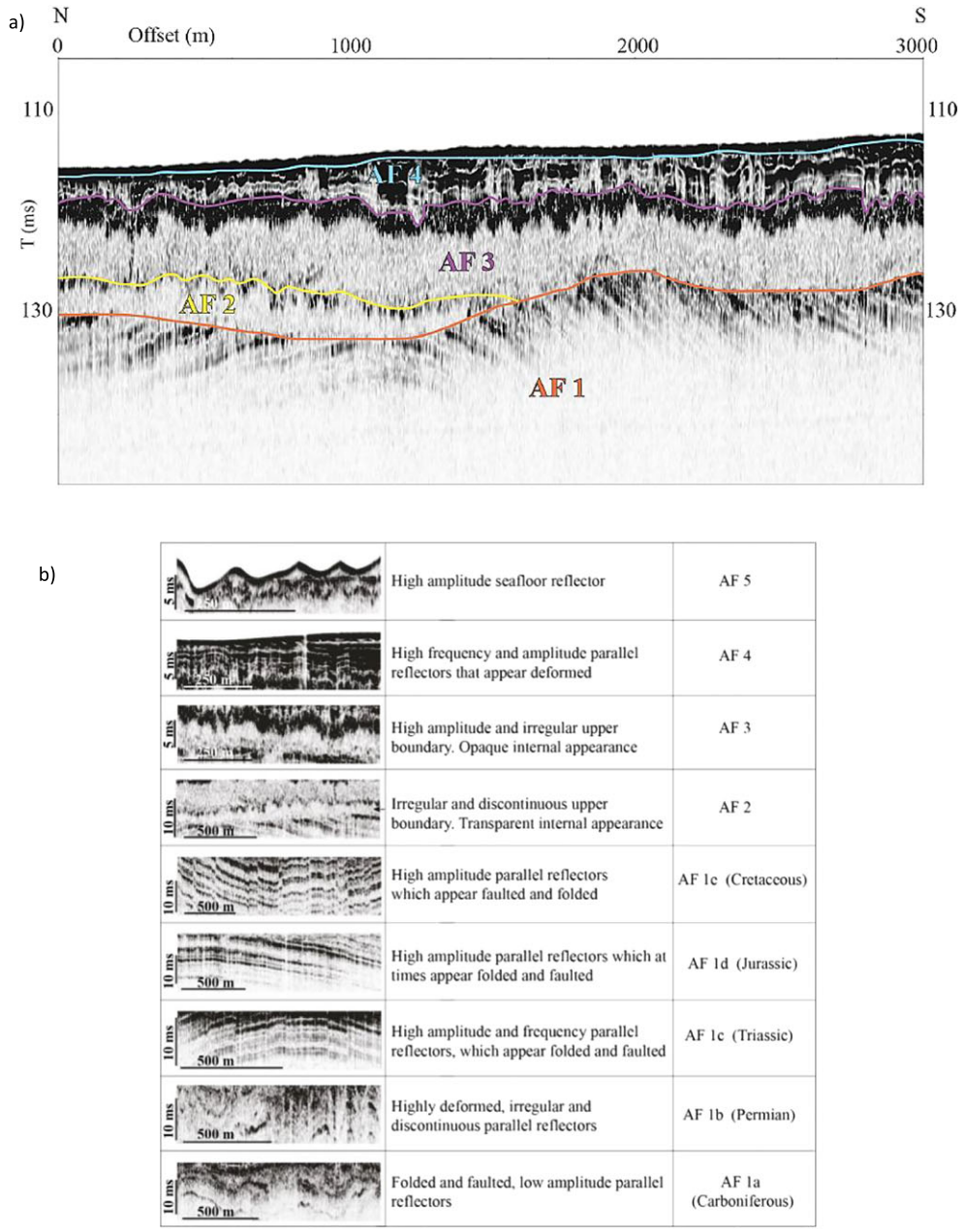

Figure 5. Acoustic facies mapped across the study area. AF1 varies with bedrock type. AF2 and AF3 are acoustically opaque and structureless, though AF2 has a slightly more transparent quality. They are plastered across the underlying bedrock. Core samples show them to be diamictic in nature. AF3 forms the core of several grounding zone wedges. AF4 is a stratified sediment package that infills local basinal topography and drapes the underlying sediments. AF5, where present, is thin and transparent. It occasional forms small sand ridges. [Colour figure can be viewed at wileyonlinelibrary.com]

Foraminifera analysis was restricted to the Fl(d) and Fm lithofacies in core 132VC. No tests were present below 209 cm. The remaining samples contained low foraminifera abundance (<150 tests per sample) with the assemblage dominated by *Elphidium clavatum* with *Haynesina obiculare* a secondary species. *E. albiumbilicatum, E. askulundi* and *E. excavatum* are also present in low abundance with *Cassidulina reniforme* appearing with minor counts at 84 cm. One radiocarbon sample from benthic foraminifera was taken at 144 cm down core, directly below the lower contact of the Dmm, within the Fl(d) unit. It returned a radiocarbon age of 19 571 ± 172 cal. BP (Figure 7(b); Table I).

Core 134VC is located just offshore from Newcastle (Figures 3(a), 4(b)) and is 4.5 m long. The core base is a massive, brown, matrix supported Dmm. It has a sandy, silty, clay matrix with abundant clasts of varying lithologies and a shear strength ranging from 20 to 25 kPa. It corresponds to AF3 as identified in the geophysical survey (Figure 6). The Dmm has some subtle stratification and a gradational upper contact to a brown/red, soft, massive clay with occasional outsize clasts (Fl(d)). This unit is colour banded, and there are occasional silt laminae, granules and clasts. It is part of AF4 (Figure 6). A disturbed layer marks the upper contact and transition to a poorly sorted, gravelly, coarse sand (Sm) with shell fragments which is gradational to a moderately sorted, silty, sand (Sm), with small shell fragments; this corresponds to AF5 (Figure 6).

Core 133VC is located 20 km south of 134VC but has very similar sedimentology. At its base (333-424 cm) it is characterised by a soft brown diamict that becomes partially stratified up core (Dms), with laminations of sorted silt/clay towards becoming more frequent towards the upper contact boundary. The Dms is sharply overlain by 2 m of a brown/reddish laminated clay/silt unit with clasts and dropstones (Fl(d)). Laminae are occasional tilted and disturbed.

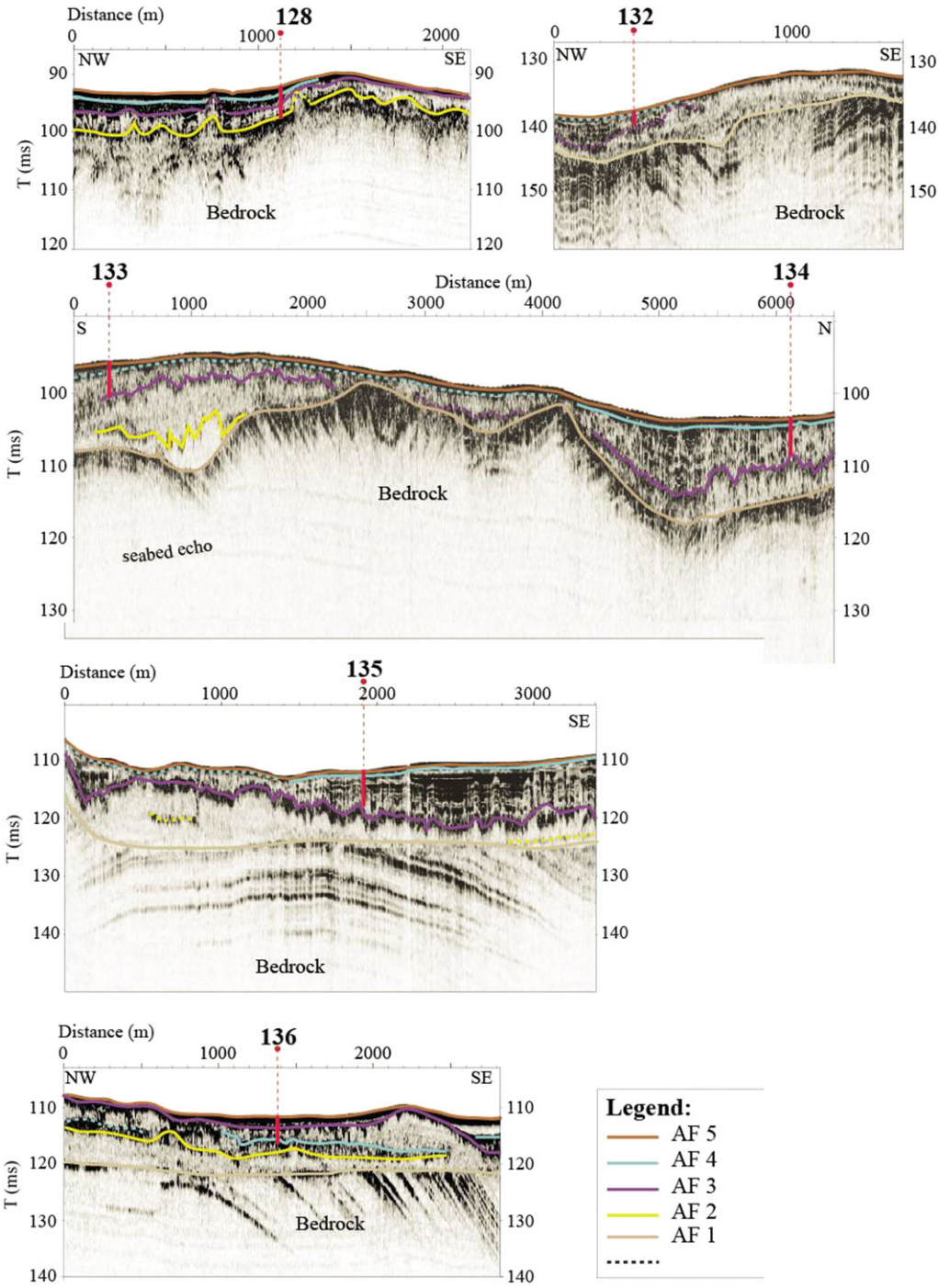

Figure 6. Acoustic facies mapped at each core location. Most cores penetrate AF4 but only just reach AF3. [Colour figure can be viewed at wileyonlinelibrary.com]

Clast abundance decreases up core and lamination becomes thinner (sub 1 mm) and more frequent; they eventually fade out. The core is capped by a shell hash and massive grey sand with shell fragments.

Core 135VC is 5.66 m long and is situated in a bathymetric low approximately 72 km east of Sunderland (Figures 3(a), 4(a), (b)). At its base is a reddish brown, massive, stiff (40–70 kPa) diamict (Dmm) with abundant clasts of different dimensions and lithologies within a silty clay matrix (Figure 8(a)). It forms part of AF4 (Figure 5). Between 494 and 488 cm there is a distinctive stratified silt unit and above this the Dmm is crudely colour banded. Overlying the Dmm is a laminated and colour banded (red/brow/grey) soft, clay silt with small clasts (Fl(d)) (Figure 8(a)). Numerous laminae (up to 1 cm in thickness) of reddish brown well sorted, fine sand (Sm) are present throughout the entire unit. This unit is part of AF 4 (Figure 6). Above the Fl(d) is an 11 cm thick, brown/grey moderately sorted, fine to medium sand layer (Sm), containing abundant shell fragments. The upper unit of the core is characterised by 23 cm of grey, moderately sorted, fine/medium sand (Sm) with shell fragments (AF5). MS data show relatively low and constant values throughout the core until a visible increase just above the top of the diamict (likely due to the presence of larger clasts; see Supplementary information).

Core 135VC was found to have foraminifera preserved within the sediment although in low abundance throughout (no foraminifera were present in the Dmm). The Fl(d) is characterised by low foraminifera abundance with the exception of a sample from 160 cm which is dominated by the species *Elphidium clavatum* plus other species such as *E. incertum, Bolivina inflata* and some planktonic species (Figure 8(b)). However, there were some notable deviations to this trend with a sample directly overlying the

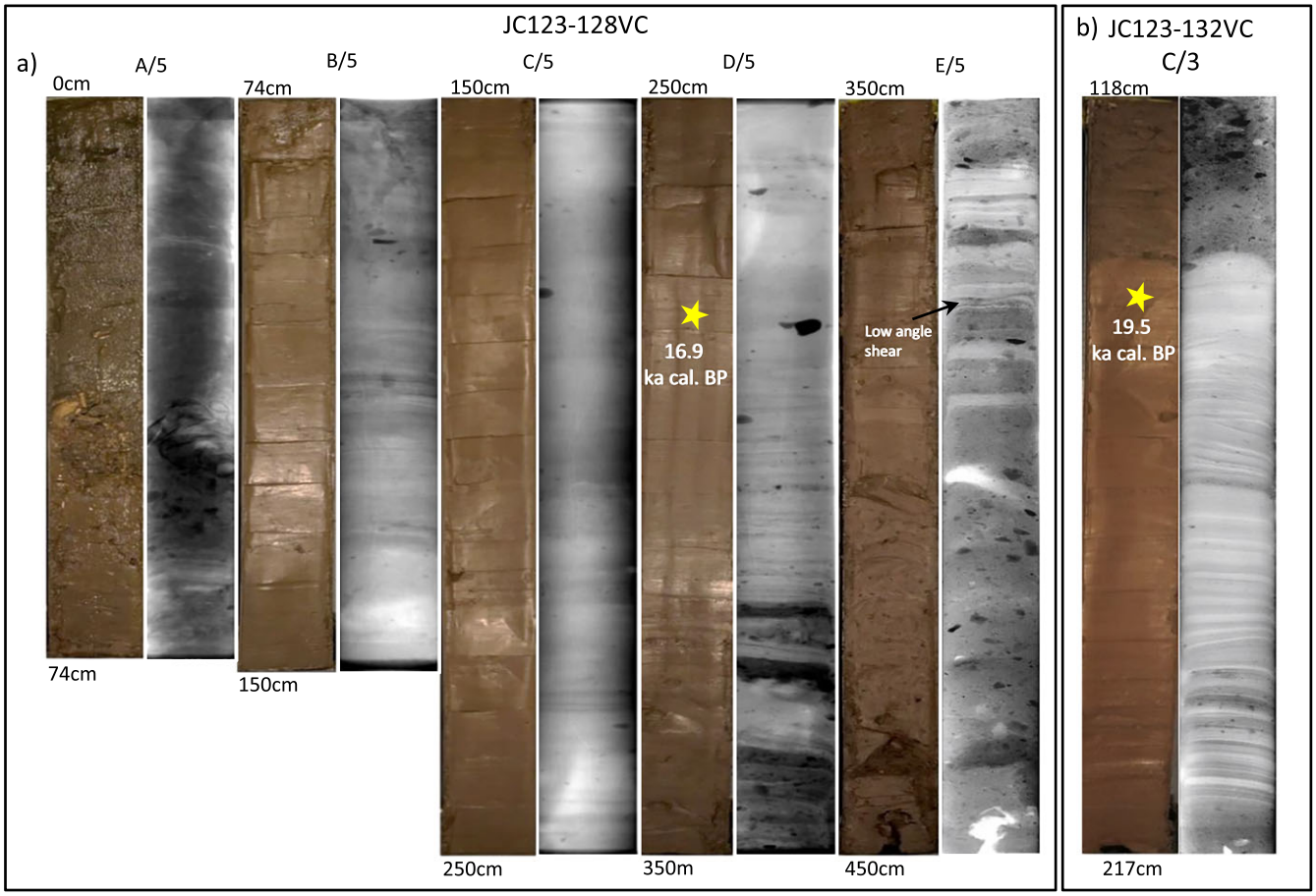

Figure 7. (a) Core JC123–128VC with paired photographs and X-ray images. The base of the core is diamictic (AF3) but grades upwards into a laminated clay/silt with a decreasing clast content (AF4). It is capped by a sandy/shelly deposit (AF5). A radiocarbon date from 280 cm down-core provided an age of 16.9 ka cal. BP. (b) Core JC123–132VC; The lower laminated sediments in this core (AF4) provide a radiocarbon age of 19.5 ka cal. BP. They are truncated by a massive diamict mid-core before grading back into AF4. [Colour figure can be viewed at wileyonlinelibrary.com]

Dmm containing *Cibicides lobatulus*, and a sample at 376 cm being composed solely of *Haynesina obiculare*. The uppermost sample was collected at 20 cm depth from within the Sm lithofacies (AF5). It contained a high abundance of quartz fragments and other grains, shell fragments and sea urchin spines, but was devoid of foraminifera.

Core 136VC is 4.05 m long and located approximately 16 km southeast of core 135VC (Figures 3(a), 4(a)). It comprises a lower unit of interlaminated sand, silts and clays (Fl/Sl) overlain by an upper diamict (Dmm) which is capped by a shelly sand (Sm). The lower Fl/Sl unit is part of AF4 has rapidly alternating laminae with several silty/sand laminae exhibiting bedforms, with planar cross lamination, micro-ripples, and micro cut and fill structures (Figure 9(a)). The contact to the overlying Dmm appears gradational and the Dmm(s) is partially stratified in places with thin, well sorted, silty lamina. It has a silt/clay matrix and shear strengths that vary between 50 and 70 kPa. The acoustic imagery from the site appears to show a lens/sheet of sediment off-lapping the north side of the local basin where 136VC is situated (Figure 4(a)). The upper 70 cm of the core is composed of a silty, coarse sand with abundant shell fragments (AF5).

Core 137VC is 5.66 m long and situated approximately 50 km northeast of 135VC. AF3 was not present at the base of the core. The lowest unit (AF4; 68–566 cm) is composed mainly of interlaminated silts and sands that fine upwards into silt and clays (Figure 9(b)). Laminae become more frequent but thinner up core. A mixed benthic foraminifera sample, with a species assemblage dominated by *Elphidium clavatum*, from 552 cm provided a radiocarbon age of 19 895 ± 218 cal. BP (UCIAMS-176372; Table I). The upper unit (0–68 cm) is a dark grey to olive grey silty coarse sand with abundant shell fragments (AF5). The contact between the two units is heavily disturbed with intraclasts of clay pointing to reworking of the lower unit.

Onshore sediments

To provide a tie point for the offshore data (both sedimentologically and geochronologically) additional evidence for NSL glaciation is also presented from Seaham where sands and gravels sit between two diamicts. This site exhibits a coastal section ~ 4 km long which has a tripartite glacial sequence sitting over Permian Magnesian Limestone. The lower diamict is dark brown, crudely stratified in places, with shear and stringer structures composed of crushed Permian limestone common towards its base (Figure 10). There are also occasional crude lenses of partially sorted gravel at the interface between underlying bedock and the diamict. Glacially abraded and striated clasts are common with a predominance of Permian Magnesian limestone, and Carboniferous limestones and sandstones. Overlying the lower diamict are up to 5 m of well sorted sands and gravels that display much lateral variability with planar-bedded, rippled, channelised and foreset bedded sands. In places the sand are deformed, over-folded and contorted. They are overlain by a laterally discontinuous upper diamict which is dark brown in colour with frequent deformed intraclasts/pods of reworked sand. Glacially abraded and striated clasts are sparse. Three sand samples from the middle sands provided very consistent OSL ages ranging from 19.1 ± 1.9 (Shfd14065) – 19.9 ± 2.3 ka (Shfd14066; Table II).

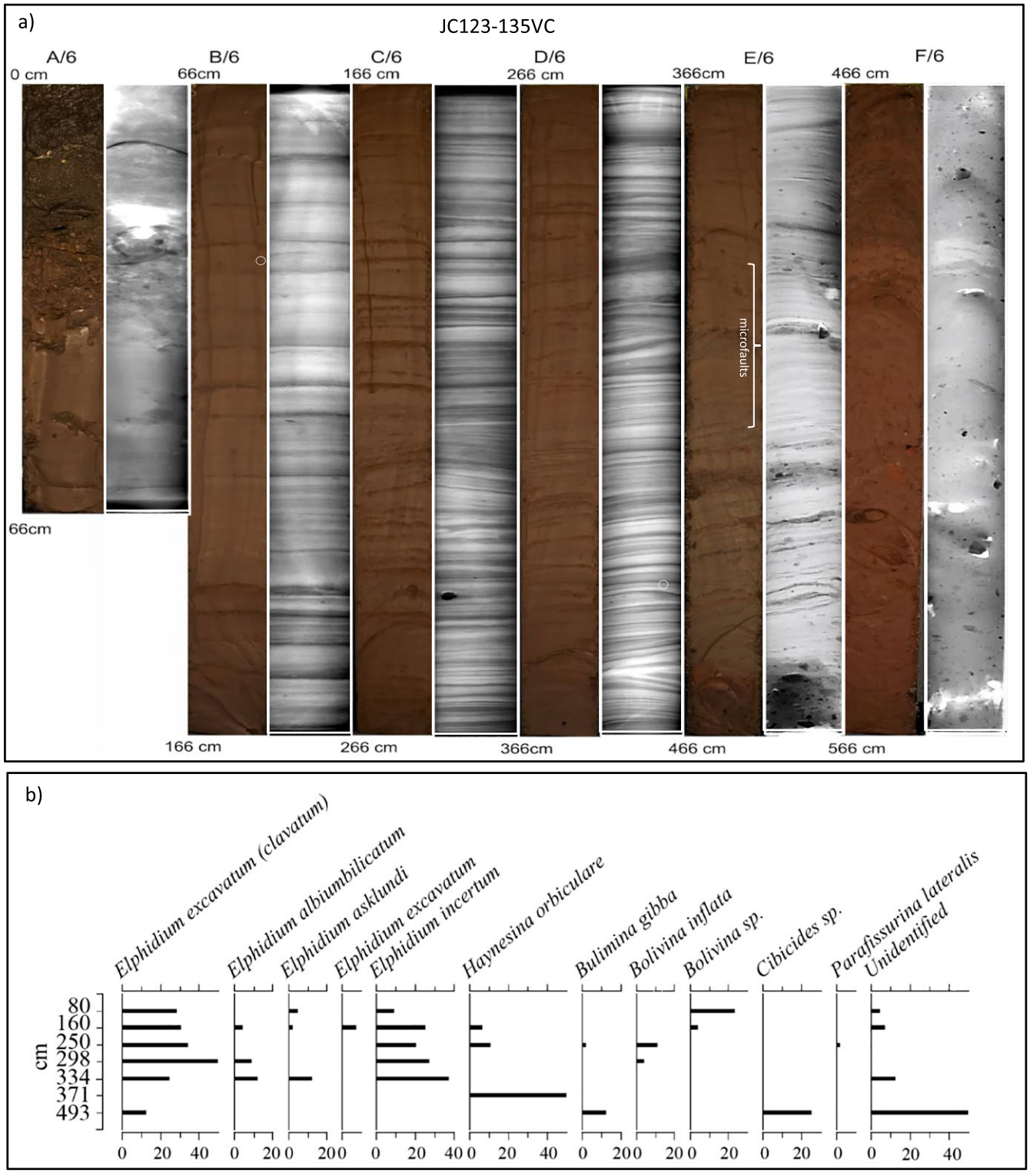

Figure 8. (a) Core JC123–135VC with paired photographs and X-ray images. This core typifies many in the study area with a lower massive diamict (AF3) grading upwards into a stratified diamict before the sediments become intensely laminated (AF4). The lack of clasts in the laminated sediments suggest a lack of ice rated input during deglaciation. The core is capped by a distinctive sandy/shelly deposit (AF5). (b) Foraminiferal counts form core JC123-135VC. *Elphidium excavatum (clavatum*) and *Cassidulina reniforme* are known indicators of extreme glacial marine environments, and other indicator species such as *Elphidium incertum, Elphidium asklundi, Elphidium albiumbilicatum, Haynesina orbiculare* and *Bolivina sp.* further corroborate cold glaciomarine conditions. [Colour figure can be viewed at wileyonlinelibrary.com]

Geomorphology of the seafloor

Bedrock ridges

Major ridges are numbered R1–R24 for ease of description and marked on both Figures 3(b) and 4(a). R1–5 generally form a series of short ridges trending NE to SW in an area underlain by tilted and folded Cretaceous rock (Figures 2(a) and 4(a)). R3 is a discontinuous ridge that can be traced intermittently over 20–30 km and follows a faulted zone of Cretaceous and Jurassic rocks cutting through the Triassic rocks to the west. R2, 4–5 form much shorter ridges typically 5–10 km in length and only 1– 3 m in amplitude. R6 is a sharp and well defined and coincides with an intrusive complex (Figure 4(a)). R7 to R9 are less prominent and formed in Triassic rock. They are partially overlain by acoustic

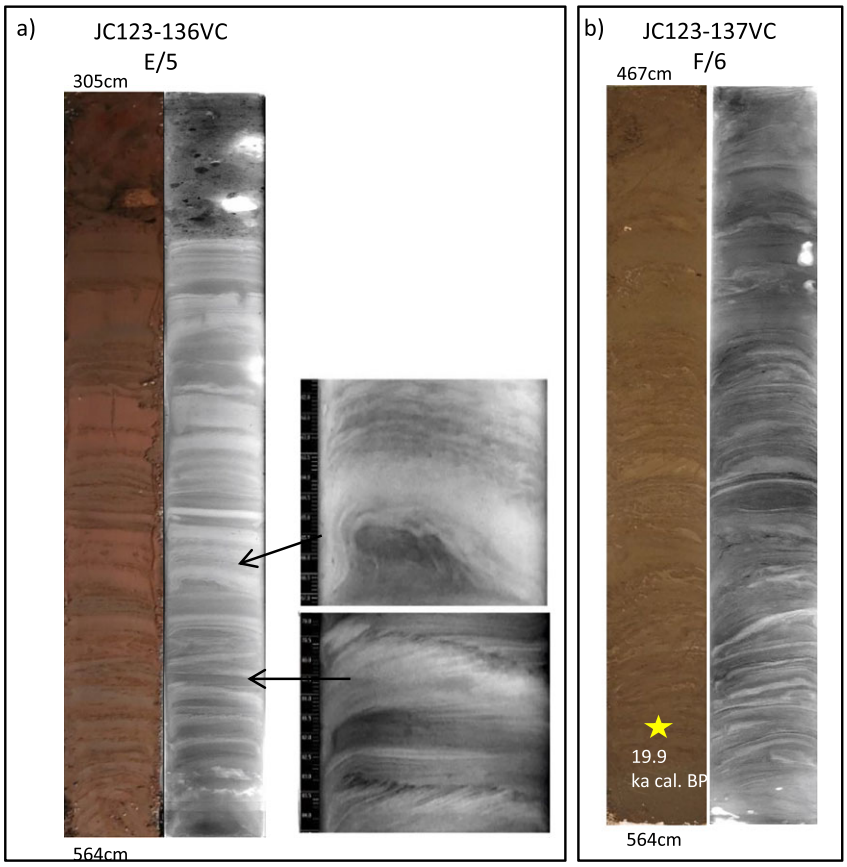

Figure 9. (a) Core JC123–136VC – the lowest section of this core exhibits clear evidence for current reworking on the seafloor cross-lamination, micro-ripples, and micro-cut and fill structures suggesting underflow activity. (b) Core JC123–137VC (see Figure 17 for locality) has a 5 m sequence of glaciomarine sediments similar in character to AF4. A radiocarbon date from the base of the core provides an early deglacial age of 19.9 ka cal. BP. [Colour figure can be viewed at wileyonlinelibrary.com]

facies AF3 which forms a broad wedge (W1) in this region of the seafloor (Figures 3(b), 4(a), (b)). R10 has very little sediment cover and is cored by Permian rocks. R11 is a very prominent ridge. It is up to 8–10 m high, up to 20 km in length (though partially discontinuous), sharp crested in places with steep slopes and occasionally rectilinear in planform. R11 is on the boundary between the Triassic inlier and the Permian rock to the north. R12 is underlain by Permian bedrock and forms more of a prominent step in the seafloor topography. R13 coincides closely with an intrusive complex mapped closer to shore to the west (Figures 2(a), 4(a)). R14-R18 are somewhat different in character to the ridges further south. They trend NE to SW but have rounded, low amplitude crests and form a corrugated pattern across the seafloor (Figures 3(a), (b), 4(a)). They coincide with the boundary between the Permian strata and Carboniferous rocks further west (Figure 2(a)). R19–R24 are small, discontinuous, sharp-crested ridges formed in Carboniferous (Dinantian) strata, and which become draped in glaciogenic sediment to the north (Figure 4(a)). It is clear from the acoustic and bathymetric data that large tracts of the seafloor are sediment deficient and floored by bedrock.

Sediment wedges and ridges

Two wedge-like features can be seen on the seafloor and are composed of sediment (W1 and W2; Figures 3, 4). Wedge 1 (W1) is ~ 30 km wide and ~100 km in length. It runs NE to SW and is ~10–15 m high. It has an arcuate planform, an asymmetric geometry and convex upper surface with small surface perturbations where bedrock ridges are close to the seafloor (e.g. R7 and R9; Figure 4(a)). In cross-profile W1 displays a long, low angle dip slope to the north (proximal) and a steep, shorter southerly (distal) slope (Figure 4(a), (b)). It is composed of acoustic facies AF3, but also incorporates basal lenses of AF2 (up to 25 m of sediment). Internal stratigraphic architecture was not discerned during cruise JC 123. Wedge 2 (W2) is smaller than W1, being ~9-12 m high, 3 to 5 km wide and ~25 km long (Figures 3, 4(a)). It has an arcuate, wedge-like planform and a strong asymmetric geometry with a steep southerly slope (distal) and longer, gentler northern slope (proximal). It is composed predominantly of acoustic facies AF3 with no apparent internal structure.

Unlike W1 and W2, the ridge marked M1 has a sinuous/multi-lobate planform that can be traced over 25 km running NE to SW across the northern part of the study area (Figures 3, 4(a)). In cross-profile it is symmetric and composed of glaciogenic sediment (AF3) that drapes Permian bedrock below. It has relatively gentle, low angle distal and proximal slopes with a distinctive central crest. There is perhaps a further section of M1 just north on R12 (Figure 3(b)).

Lineations

Elongate and narrow lineations are common in the central part of the study area (Figure 3). Most run northwest to southeast. They vary in planform; most are straight, but they can also be curved, sinuous and occasionally bifurcate. There is also a distinct sub-population that display an offset pattern with a northeast to southwest orientation (Figure 3(b)). The length of the ridges spans from a few hundred meters up to ~10 km. Widths vary from tens to a few hundred meters, averaging 300–500 m in width. Elongation ratios vary between 3:1 to 14:1. They rarely exceed 2 to 4 m in amplitude but this is dependent on sediment cover. Where Holocene sediment cover is sparse they have well defined steep slopes and rounded crests (Figure 11(a)). Where sediment drapes are slightly thicker their surface form is more subdued (Figure 11(b), (c)). Many of the streamlined bedforms

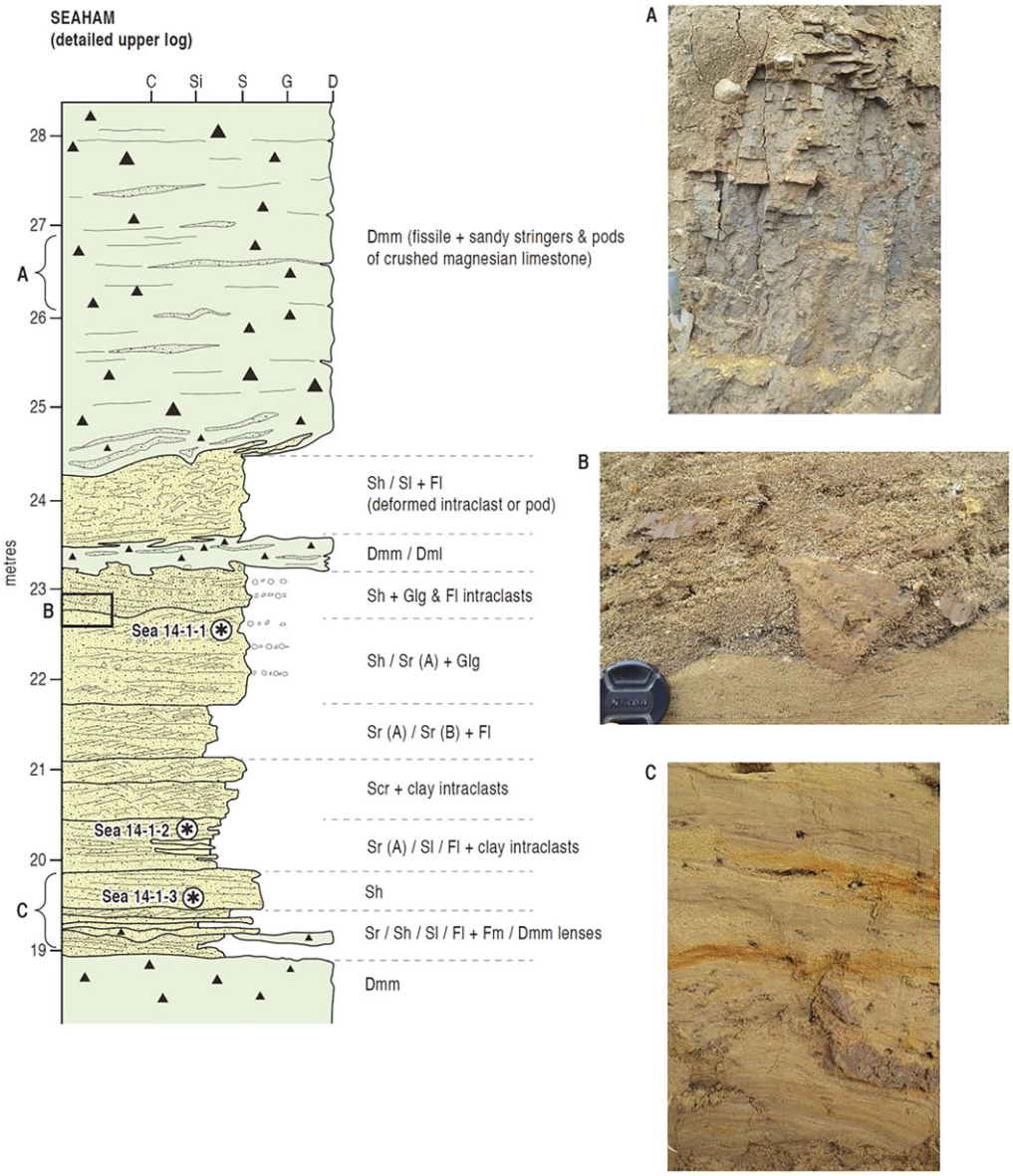

Figure 10. Glacial stratigraphy from a coastal section at Seaham, County Durham. The section has two glacial diamicts separated by a glacial fluvial sand. These sediments cannot be directly related to the offshore acoustic stratigraphy as the near shore areas have been scoured of glacial sediment, but glaciofluvial sands provide three OSL ages that limit final deglaciation of the coast by the NSL to after 19.6 ka. [Colour figure can be viewed at wileyonlinelibrary.com]

have a bedrock core forming the nucleus but there are examples where sediment (AF3) constitutes part of, or in rare cases, the whole bedform (Figure 11(c)). In the west of the study area, data collected by the British Gelogical Survey in 1993/4, also shows streamlined bedforms buried beneath the seafloor. They are approximately 2–3 km long and 3–5 m in amplitude and appear to be constructed from AF3 (Figure 11(d)).

When imaged at high resolution many of the bedforms appear to be seeded from perturbations on the seabed and are slightly tapered in that they are wider to the north and narrower to the south. It is also possible to see that some ridges are more ovate in planform (Figure 12). Streamlined bedforms are sparse over W1. Indeed, they may be partially buried by W1 and it is clear from both the seafloor geomorphology (Figure 3(a)) and acoustic data (Figure 4) that the bedrock surface in this area is buried by a significant sediment cover (AF3).

Channels

Several large channels can be seen in the northern half of the study area. Many of the depressions are narrow, elongate and have low sinuosity. They are generally orientated NW–SE (Figure 3). C1 is a broad flat channel that terminates close to R13. C2 is a well-defined single channel (Figure 13(a)). C3 is a more complex system having a single channel north of M1, but appearing to split into C3 and C4 south of M1, before joining again and bending southwestwards. The main segments of C2 and C3 are over 20 km long. Their width varies between ~400 and ~2700 m wide. In cross-profile, they are mainly V-shaped and in long profile are irregular with undulatory long profiles (Figure 13(b), (c(). In places they are incised up to ~16 m deep into the seafloor. C5 is a more complex channel being formed of a series of partially disconnected segments and bends. There are also several small, highly sinuous channels superimposed on R11 (Figure 12).

Interpretations and Implications

The glacial imprint of the NSL offshore from the east coast has several distinctive elements. These include transverse bedrock ridges, subglacial channels, streamlined glacial lineations and till wedges. Together these form a mixed-bed glacial

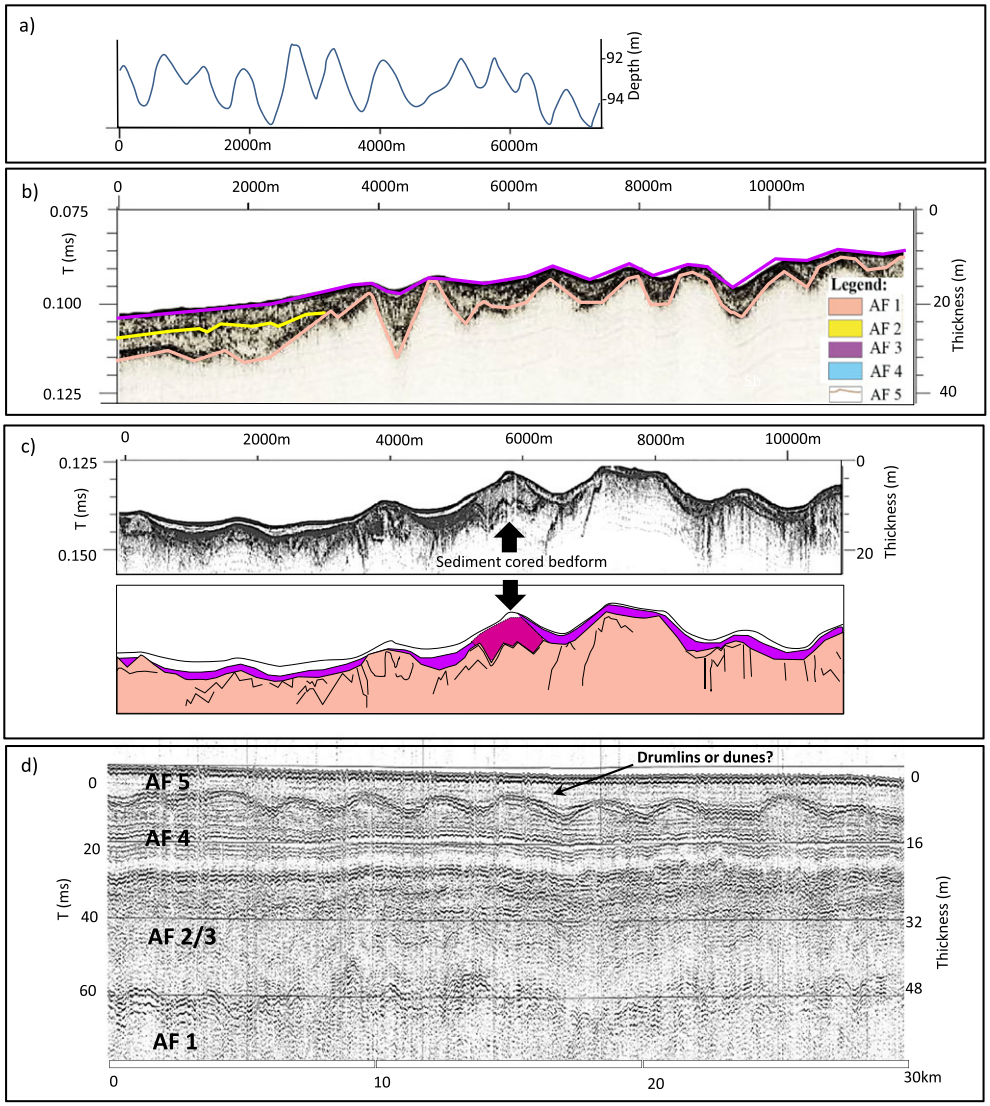

Figure 11. (a) A bathymetry cross-profile across a series of mega-scale glacial lineations. Drift/bedrock cores not differentiated. (b) Partially buried bedrock ridges. Where drift is slightly thicker their surface form is more subdued. (c) In some localities glaciogenic sediment constitutes the whole bedform forming drumlins (pink = bedrock; purple = diamict AF3; fuschia = drift drumlin core. (d) BGS seismic line 1993-1/1close to the Northumberland coast. Note the buried streamlined bedforms. The have drumlin-like dimensions but have been previously interpreted as buried dunes by Brew (1996). [Colour figure can be viewed at wileyonlinelibrary.com]

landsystem signature formed through glacial erosion (abrasion, streamlining and plucking), subglacial sediment deposition, subglacial meltwater excavation and, finally, deglacial glaciomarine sedimentation.

Bedrock influence on seafloor geomorphology

Transverse bedrock ridges trending NE to SW are prominent across the seafloor and formed in Carboniferous, Permian and Triassic rocks. In the north, the orientation of ridges R14 to R24 is controlled by the NE/SW axial orientation of synclines and anticlines in the Carboniferous strata (Figure 14). R11–R13 also trend NE/SW but they lie within a zone of Permian strata with a Triassic inlier. They are not related to the large synclinal basin forming the Triassic inlier, but could be controlled either by faults or regional igneous intrusions that run SW/NE from the coast towards the east (Figure 14; e.g. Whin Sill). R7 to 10 are underlain by Permian and Triassic rocks but their relationship to the regional structural geology is unclear. However, R6 is clearly intrusive, lying close to the geological boundary between the Jurassic and Permian rocks (Figures 4(a), 14). R1–R5 trend NE to SW in an area underlain by tilted and folded Cretaceous rock (Figure 4(a)), but R3 follows the fault bounded contact between the Cretaceous and Jurassic rock that trends westward (Figure 14).

The bathymetric data suggest that the majority of bedrock ridges and surfaces in the study area are smoothed and abraded. There are occasional patches of bedrock that have 'rough' surfaces (e.g. see bedrock surfaces below core sites 133VC and 134VC; Figure 6) but this is likely a product of the acoustic amplification of sub-vertical bedrock structure rather than a signal of plucking and quarrying. North of W1 the seafloor morphology is primarily controlled by the bedrock structure with secondary glacial streamlining of drift, which has resulted in a patchy subglacial mosaic of glaciogenic deposits and exposed bedrock (e.g. Eyles and Doughty, 2016; Figure 3(a)). North of R12, bedrock close to the seafloor and a thin drift cover has resulted in a relatively high bed roughness (Figure 13).

The channels that run through the area north of R12 are clearly subglacial in origin as they have undulatory long profiles that signify water flowing under high pressure in Nye or tunnel channels (Figure 13; e.g. Booth and Hallet, 1993; Ó Cofaigh, 1996; Clayton *et al.*, 1999; Praeg, 2003). They perhaps formed when the ice margin was close to R12, and their NW to SE trajectory supports regional ice flow towards the southeast

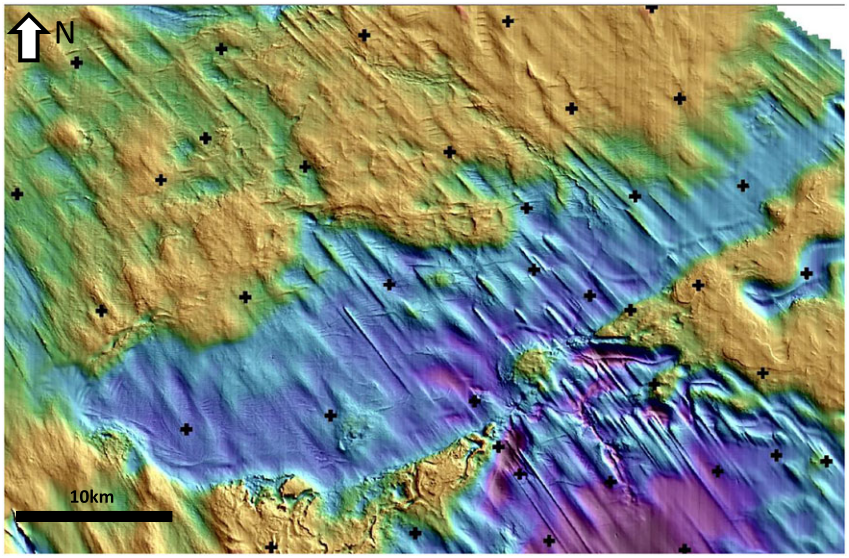

Figure 12. Streamlined bedforms in drift across the seafloor north of core 132VC. Some, but not all, bedforms appear to be seeded from perturbations on the seabed. It is also possible to see that some ridges are more ovate in planform. Yellow areas are bedrock highs with very thin glacial sediment cover. See Figure 3 for locational information. [Colour figure can be viewed at wileyonlinelibrary.com]

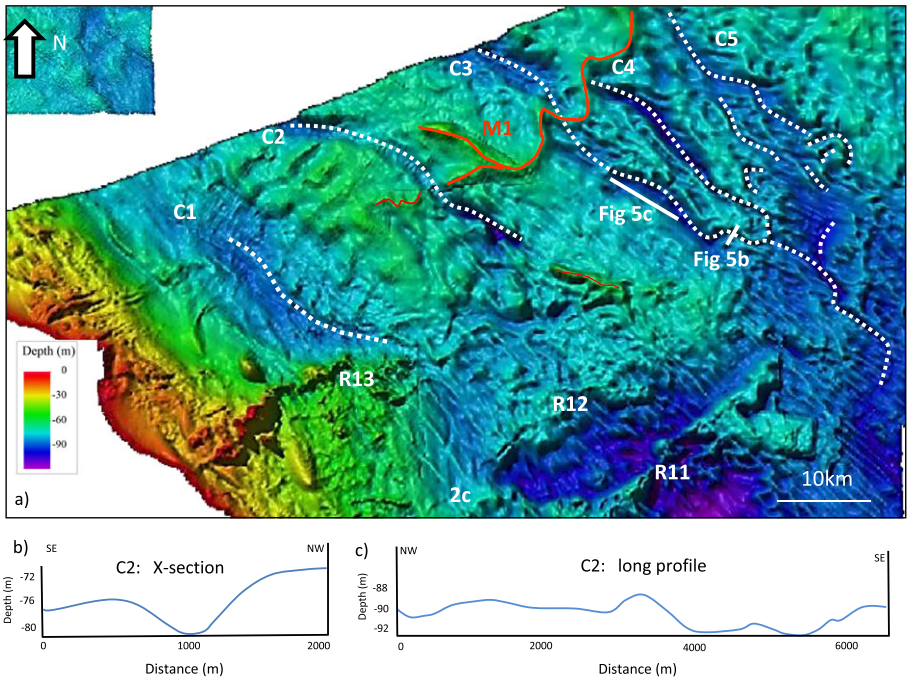

Figure 13. (a–c) Distinctive channels cut into bedrock in the northern part of the study area running NW to SE (parallel to former ice flow direction). C3–C5 are anastomosing and interconnected. C2 is up to 10 m deep and has an up/down long profile. [Colour figure can be viewed at wileyonlinelibrary.com]

because subglacial water flow tends to broadly follow the regional ice sheet surface gradient (cf. Shreve, 1972; Booth and Hallet, 1993). The cutting of these channels into bedrock has further enhanced overall bed roughness/bumpiness of this area of the seabed in the area north of R12.

Subglacial sediment and landform genesis

The seismic data across the study area shows five distinct acoustic facies (Figures 4, 5; AF 1–5). AF1 can be clearly identified as bedrock but AF2 and AF3 have characteristics similar to subglacial diamicts. AF2 is thin and patchy with variable thickness (~2–6 m). In contrast, AF3 forms distinctive, discontinuous sheets across the study area and has an average thickness of ~4–10 m. It can thicken to 15–20 m where it forms the wedges. Both AF2 and AF3 have high amplitude and highly irregular upper reflectors and are mainly acoustically transparent with little internal structure. AF3 also occasionally has chaotic internal reflectors. MS measurements range from 100 to 629×10^{-5} SI probably due to differences in grain sizes and the concentration of magnetic minerals (Kilfeather *et al.*, 2011; Hogan *et al.*, 2016). Such acoustic properties have previously been interpreted as subglacial tills (Cameron *et al.*, 1992; Gatliff *et al.*, 1994; Huuse and Lykke-Anderson, 2000; Dove *et al.*, 2017), with the heterogeneous nature of diamictic

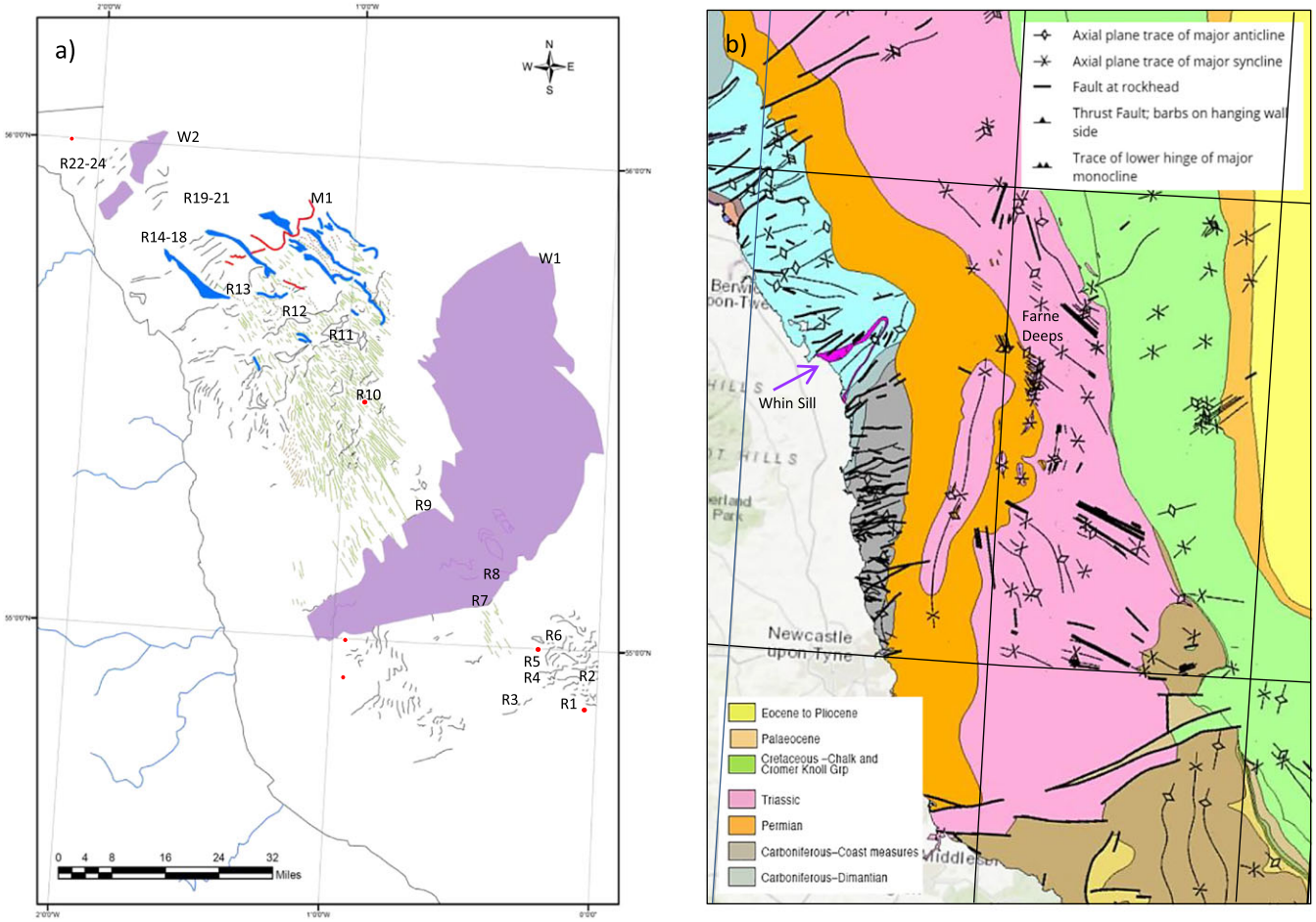

Figure 14. Bedrock geology offshore from Durham/Northumberland showing the structural geology of the region compared with the distribution of glacial landforms. Transverse bedrock ridges trending NE to SW are prominent across the seafloor and formed in Carboniferous, Permian and Triassic rocks. They are controlled by orientation of synclines, faults or regional igneous intrusions. MSGL occur mainly occur Permian and Triassic bedrock but the juxtaposition of both bedrock-cored and sediment-cored bedforms reinforces the notion that in areas of thin sediment cover the subglacial bed is partially emergent and partially inherited with bedforms evolving via a combination of erosion, deposition and deformation. [Colour figure can be viewed at wileyonlinelibrary.com]

sediments resulting in acoustic homogeneity when observed in seismic profile (Hogan *et al.*, 2016).

Cores 128VC, 133VC, 134VC and 135VC confirm this interpretation and all have diamictic sediments that were recovered from the top of AF3 (Figure 6). From the core data, AF3 is predominantly massive, though occasionally partially stratified towards its upper contact. These diamicts are characterised by abundant clasts dispersed in a soft clay-silt matrix. Shear strength measurements for these facies range between ~11 and 70 kPa, which are lower values than reported for many subglacial tills (Boulton and Paul, 1976; Iverson *et al.*, 1994; Clarke, 2005; Iverson, 2010), but similar shear strengths have been described from the West Antarctica continental shelf where soft subglacial diamicts are often associated with mega-scale glacial lineations (MSGL) (Dowdeswell *et al.*, 2004; Ó Cofaigh *et al.*, 2005; Evans *et al.*, 2005; Kilfeather *et al.*, 2011).

Foraminifera specimens were not found in all the diamictic units sampled, which also supports a subglacial origin, but the upward shift to partially stratified diamict in many of the cores suggests that these sediments are transitional from subglacial to proximal glaciomarine diamicts (e.g. Figures 7(a), 8(a)). The partially stratified and laminated silts and clays found within the upper parts of AF3 thus represent intermittent and gradual changes from subglacial deposition to processes dominated by undermelt, underflow/turbidity currents, ice rafted sediment, subaqueous debris flow and suspension settling (Gravenor *et al.*, 1984; Hart and Roberts, 1994; Ó Cofaigh *et al.*, 2005; Hogan *et al.*, 2016). Possible low angle faults/shears in the diamict in 128VC (Figure 7(a); section E/5) and minor disturbance and deformation of laminated units towards the top of AF3 (see Figure 8(a); core 135VC; section E/6) hint at minor lateral stress transfer through the sediment and subglacial/submarginal deformation of the sediment pile.

AF3 has been previously mapped as Wee Bankie Formation in the western NSB (Figure 2(b)). It has been described as having a patchy distribution and being interspersed with bedrock exposures. Clast lithologies within it indicate a Scottish provenance (Cameron *et al.*, 1992; Gatliff *et al.*, 1994; Carr *et al.*, 2006; Davies *et al.*, 2011) and it is contiguous with the Bolders Bank Formation further south (Figure 2(b)). Both formations therefore relate to the advance of the NSL, but due to the time-transgressive nature of glacier erosion and deposition (cf. Boulton, 1996a, 1996b), the Bolders Bank Formation is a 'down-ice' subglacial lithofacies produced via the net advection and thickening of subglacial till towards the southern margin of the NSL (Dove *et al.*, 2017; Roberts *et al.*, 2018), whereas the Wee Bankie Formation is a later subglacial lithofacies deposited as part of an active subglacial assemblage as the NSL retreated northwards.

Across the study area AF3 is found in association with glacial lineations and sediment wedges, supporting a subglacial/submarginal origin (Clark, 1993; Stokes and Clark, 2001; Evans and Hiemstra, 2005). To the south of R11, the deepest areas of the seabed coincide with the synclinal Triassic inlier that runs

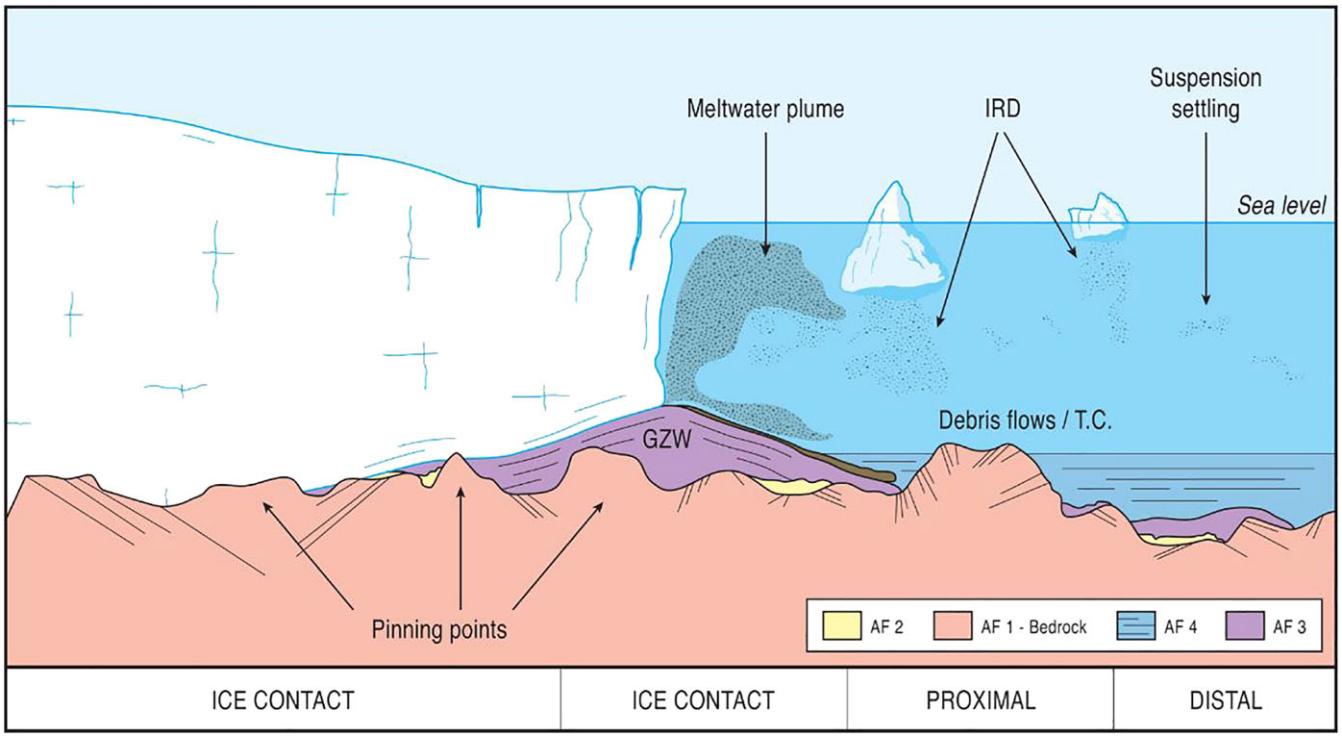

Figure 15. Mixed-bed glacial landsystem of the NSL during deglaciation under marine conditions. An irregular, scoured and eroded bedrock surface forms the base of the sequence. Subglacial sediments form discontinuous till sheets which feed grounding zone wedges. These are later draped by proximal and distal glaciomarine sediments as the margin actively retreats. The presence of an ice shelf is, as yet, unsubstantiated. [Colour figure can be viewed at wileyonlinelibrary.com]

south-southeast towards Newcastle (Figure 14). This area is heavily lineated and streamlined southwards towards W1 where the lineations dissipate and are perhaps buried beneath the wedge. Based on their shape and dimensions these bedforms are a mixture of drumlins and MSGL (Ely *et al.*, 2018), and are composed of both hard and soft bed landforms. The elongate and narrow bedforms in the area between R11 and W1 vary in length from a few hundred meters up to ~10 km and in width from tens to a few hundred meters (~ 300– 500 m). Amplitudes are ~ 2–4 m and their elongation ratios vary between 3:1 and 14:1. They are analogous to MSGL mapped in other formerly glaciated regions (Clark, 1993, 1994; Stokes and Clark, 2002; Spagnolo *et al.*, 2014; Ely *et al.*, 2018). Figure 11(a) displays the cross profile form of the MSGL on the seafloor but it is difficult to be certain whether they are bedrock or till cored. To the immediate east of R10 and R11 the MSGL appear to closely coincide with the axial orientation of multiple small-scale synclines and anticlines mapped within the Triassic sequence associated with the Farne Deeps (Figure 14). In other areas, the MSGL appear to bifurcate and anastomose. The sub-population in Figure 3(b) that exhibit an offset pattern (northeast to southwest orientation) perhaps relate to bedrock influence sub-parallel to the main synclinal axis of the Triassic inlier (Figure 14). Other lineations (marked as minor bedrock ridges; Figure 3(b)) are very sinuous suggesting bedrock influence. There is also the possibility some could be eskers but this requires further investigation.

There are clear bedrock cores in streamlined bedforms to the immediate south of R11 (Figure 11(c)). These bedforms are slightly more ovate and drumlinoid in planform (Figure 3(a)) but they have bedrock cores with glaciogenic material mainly concentrated in the lows between bedforms. The MSGL south of 132VC display a thin veneer of glaciogenic material (AF3) over bedrock bumps in the north but, as drift thickness increases southward (Figure 4(b)), the upper surface of AF3 becomes streamlined (drumlinised) and the influence of bedrock perturbations is reduced. Slightly further west, seismic records acquired by the BGS (1993-1-1) also possibly show buried streamlined drumlins, though they have previously been interpreted as subaqueous dunes formed by tidal currents (Brew, 1996; a theory somewhat incompatible with ice sheet retreat under glaciomarine conditions; see below) (Figure 11(d)). However, to the immediate east of core 134VC bedrock again forms the core of large, moulded, bedrock hills on the seafloor (Figures 3(a), 4(b)). Hence, it is a combination of sediment distribution and thickness (plus bedrock roughness), that controls bedform-type and position in relation to regional ice flow; as well as determining the patchiness of the glaciogenic sediment cover in this upstream part of the NSL.

When imaged using high-resolution bathymetry many of the MSGL have seed points, suggesting that bedrock knobs are close to the surface and trigger bedform initiation, with pervasive deposition and deformation of subglacial till being contemporaneous with the evolution of the MSGLs (cf. Boulton, 1971, 1975, 1976, 1982, 1987; Jansson and Kleman, 1999; Stokes *et al.*, 2014; Spagnolo *et al.*, 2014). North of R12 there only are a few MSGL, suggesting thin sediment cover over the bedrock, however, the MSGL are better developed where sediment is thickest between R12 and R11 and south of R11 (see Figure 4(a) between R10 and R13 and Figure 12). The complete lack of MSGL over R11 (see Figure 12) shows there is little subglacial sediment over this ridge. The juxtaposition of both bedrock-cored and sediment-cored bedforms further reinforces the notion that in areas of thin drift cover the subglacial bed is partially emergent and partially inherited, with bedform assemblages both evolving and hybridised via a combination of erosion, deposition and deformation (Clark *et al.*, 2010, 2018; Eyles *et al.*, 2016). Many of the MSGL in the central study area (Figure 12) are pinned to bedrock bumps or initiator scarps and, thus, their position and distribution is a function of both bedrock morphology and sediment supply.

W1 and W2 (Figures 3 and 4) are clearly grounding zone wedges (GZW) (Powell, 1990, 2003; Ottesen and Dowdeswell,

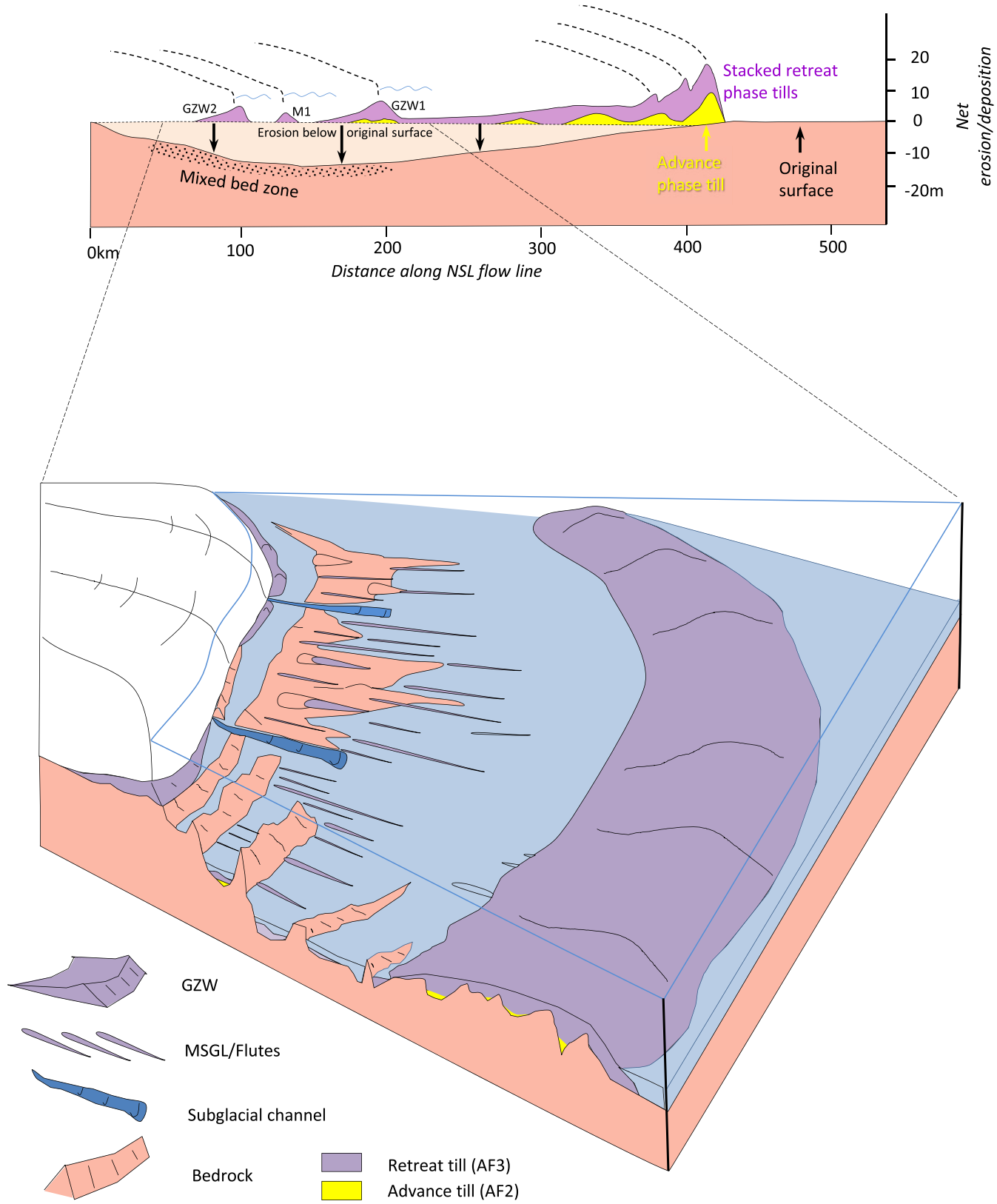

Figure 16. The NSL imprint in this region has characteristics of both hard and soft bed processes; it is a mixed-bed subglacial landsystem. It is a product of an ice stream lobe undergoing rapid transition from a terrestrial piedmont-lobe margin with a net surplus of sediment to the south, to a dynamic, quasi-stable, tidewater margin as the ice withdrew northwards. Grounding line instabilities, drawdown and enhanced flow velocities triggered by marine inundation of the North Sea would have been the most influential feedbacks controlling the development of the mixed-bed signal during deglaciation; bed excavation to partial bedrock, increasing bed roughness, till advection and GZW construction all being the knock-on effects of grounding line instability. [Colour figure can be viewed at wileyonlinelibrary.com]

2006; Batchelor and Dowdeswell, 2015). They are asymmetric sedimentary depo-centres with distinctive wedge geometries, associated with the accretion of subglacial material at the grounding line of the NSL as it has receded northwards (Figures 15, 16). From the acoustic data in can be seen that both W1 and W2 are composed of AF2 and AF3 but they lack clear internal structure. Neither is well streamlined, but the association of MSGL positioned upstream of W1 suggests that the

net flux of subglacial material via bed deformation and MSGL formation was critical to the construction of a large GZW (Anderson and Bartek, 1992; Powell and Domack, 1995; Ó Cofaigh *et al.*, 2005; Ottesen *et al.*, 2007; Batchelor and Dowdeswell, 2015).

Dove *et al.* (2017) have recently demonstrated that the NSL underwent a series of quasi-stable oscillations during recession, depositing a series of superimposed, lobate-shaped till wedges offshore from Norfolk and Yorkshire. This pattern of repeated oscillation, till sheet deposition and incremental thickening has been mapped also onshore along the Yorkshire coast by Boston *et al.* (2010) and Evans and Thomson (2010), but the exact mechanisms and timing of emplacement of W1 and W2 are more difficult to discern. W2 is constructed exclusively of AF3 with no discernible internal architecture. W1 has discontinuous lenses of AF2 overlain by AF3, suggesting the emplacement of one till sheet over the other. This suggests that the ice margin was stable and receiving a net surplus of subglacial material for some time, but it is difficult to establish the exact processes that formed W1 and W2 without more detailed acoustic stratigraphy. W1 is much larger than W2, which could imply a more prolonged still-stand, but without an improved knowledge of sediment flux rates, or a better constrained chronology, this cannot be substantiated.

There is evidence for an additional still-stand/re-advance event as ice retreated north of W1 in the form of M1, which has a very different planform to W1 and W2. Its multi-lobate nature is similar to a terminal/push moraine complex (Figure 3; Dredge and Cowan, 1989; Patterson, 1997, 1998; Colgan, 1999; Evans *et al.*, 2008, 2014; Colgan *et al.*, 2003; Kovanen and Slaymaker, 2004). This may simply represent a shorter-lived event than those that constructed W1 and W2, and thus the distinctive imprint of a lobate ice margin has been preserved on the seafloor and not been obscured by the continual net advection of sediment to the ice margin (to form a more substantive till sheet/wedge).

Temporary standstill of the ice margin in order to form the GZW's may have been both internally and externally controlled. Changes in bed configuration (there are multiple bedrock highs forming pinning points below W1; Figures 4 and 15) or water depth at the margin (e.g. as sea-level increased) are two probable mechanisms that influenced grounding line stability (Powell and Alley, 1997; Schoof, 2007). Changes to ice dispersal centres and shifting ice divides over Scotland and the northern North Sea would also have been important in determining the flow behaviour of ice flowing offshore through the Firth of Forth and into the NSL during regional deglaciation.

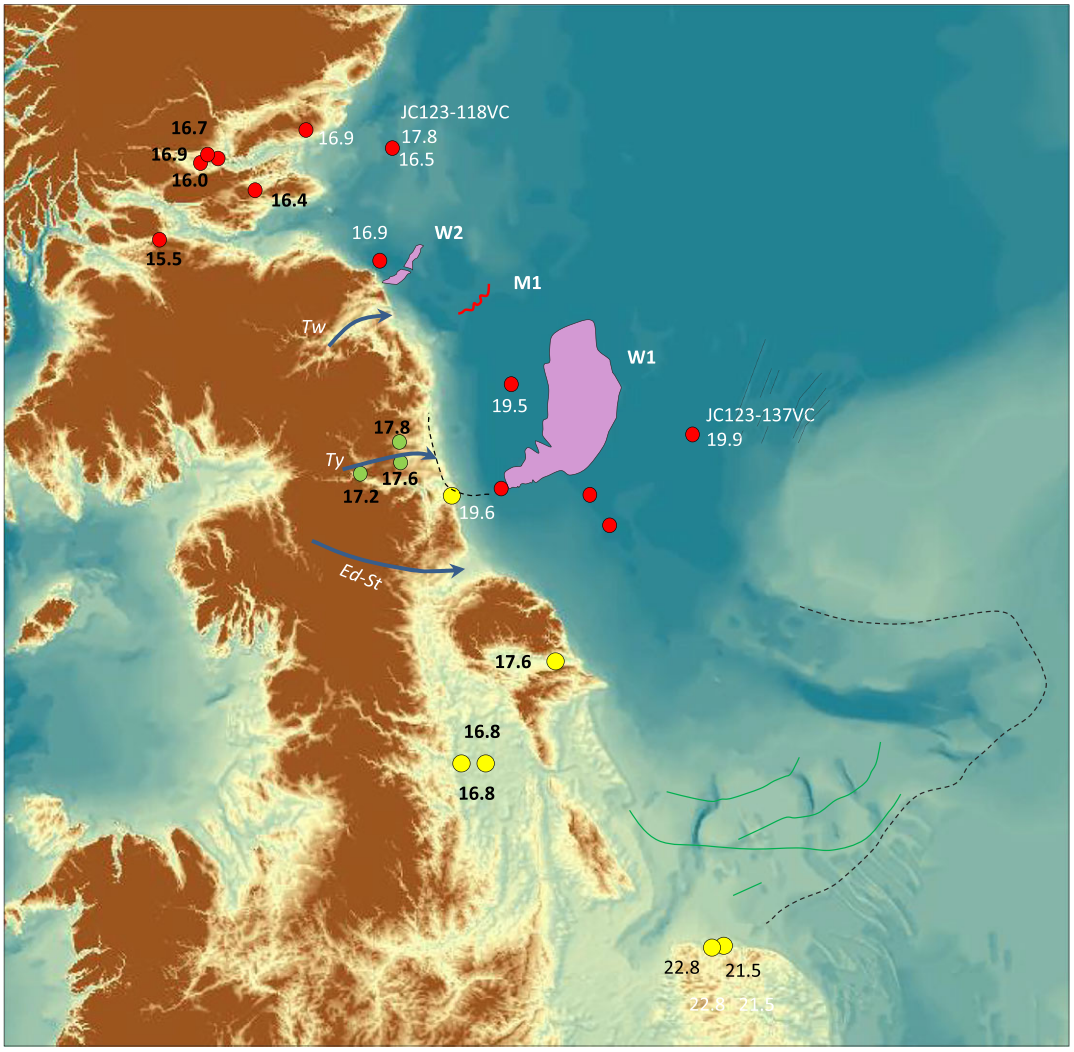

Figure 17. The retreat of the NSL based on new and existing radiocarbon and OSL ages from the east coast of the UK and the offshore areas of Durham and Northumberland. The NSL departed the north Norfolk coast after 22.8–21.5 ka BP, leaving till wedges and arcuate moraine complexes on the seafloor as it migrated northwards (green lines; Dove *et al.*, 2017; Roberts *et al.*, 2018). New dates from the Durham area and offshore suggest the ice margin became quasi-stable as a large grounding zone wedge developed (W1) at some time around 19.5–19.9 ka. W2 and moraine complex M1 also suggest further periods of ice marginal stability before the NSL retreated into the Firth of Forth between 17.8 and 16.0 ka cal. BP. [Colour figure can be viewed at wileyonlinelibrary.com]

Table III. Calibrated radiocarbon ages from the periphery of the Tay and Forth estuaries. With the exception of the site at Shiells all sites mark the onset of glaciomarine conditions with ice receding westward and onshore (note no adjustment for marine reservoir) (see Hughes *et al.*, 2011 for overview)

Site	Lab code	Geological context and material dated	Calibrated age (no mar res correction)	± error	Source
Shiells	SRR-391	Terrestrial ice free conditions; organics	16,444	205	Peacock and Browne, 1998; Harkness and Wilson, 1979
Gallowflat	AA-37787	Errol BedsFm; -Glaciomarine; *Rabilimis mirabilis* and *Heterocyprideis sorbyana*	16,693	132.5	Peacock, 2002
Gallowflat	Beta-111508	Errol Beds Fm; Glaciomarine; *Portlandia arctica*	16,000	130	Peacock, 2002
Gallowflat	CAMS-77912	Errol BedsFm; Glaciomarine; Benthic foraminifera	16,786	137.5	Peacock, 2002
Barry Clay Pit	OxA-1704	Errol Beds Fm; Glaciomarine; Balanus sp.	16,898	273.5	Peacock and Browne, 1998; Hedges *et al.* 1989
Kinneil Kerse	OxA-1347	Kinneil Kerse Fm overlying Errol Beds Fm; Marine; *Nuculana pernula*	15,488	190 -	Hedges *et al.*, 1989; Peacock 1999

What is clear from the imprint of W1, M1 and W2 is that the NSL was behaving as a piedmont lobe flowing NW to SE during overall northwards recession. The glacial imprint offshore of County Durham and Northumberland does not support the action of a defined ice stream trunk zone (with lateral shear margins; Stokes and Clark, 2001; Golledge and Stoker, 2006), nor does it provide any evidence for the eastward extensions of the Tweed or Tyne Gap Ice streams during the early phases of the LGM (Davies *et al.*, 2009; Livingstone *et al.*, 2015).

The NSL therefore, does not exhibit the classic features associated with ice stream onset zones such as convergent flow patterns, distinct lateral shear margins or a trunk zone (Stokes and Clark, 2001), however, it does share some the hard/mixed, streamlined bed characteristics described from other former ice onset zones sourced from upland Britain (e.g. Minch Ice Stream and Hebridean Ice Stream; Bradwell *et al.*, 2007; Bradwell, 2013; Bradwell and Stoker, 2015; Dove *et al.*, 2015; Krabbendam *et al.*, 2016) and Scandanavia (Ottesen *et al.*, 2016). The onset zone of the Minch Ice Stream in particular, where both soft-bed and hard-bed subglacial landform assemblages in the central and inner parts of the Minch mark grounded fast-flowing ice and a high degree of ice-bed coupling is very similar to the glacial landsystem reported herein. The transition from scoured and streamlined bedrock terrain to MSGL has also been used to infer an increase in ice flow velocity as ice passes from hard to soft bedded substrates in other ice stream onset settings such as the Hebridean Ice Stream and Norwegian Channel ice Stream (Dove *et al.*, 2015; Ottesen *et al.*, 2016). In our study area, MSGL do occur in a specific zone south of the bedrock dominated terrain between R11–18 and north of W1 (Figure 3(b)) possibly reflecting a period of ice streaming to an ice margin at W1.

Upstream of the study area direct evidence for ice stream onset within the Firth of Forth has been established by Golledge and Stoker (2006) who demonstrated that areas to the north of the Firth of Forth formed the Strathmore Ice Stream flowing northeastward. In addition, other recent work along the southern shore of the Firth of Forth also indicates preferential westerly ice flow directly feeding the NSL (Hutton, 2018). On balance therefore, it seems logical that the mixed-bed subglacial landsystem and GZWs identified beneath the NSL are clear evidence of an ice stream lobe operating along the southern edge of the Firth of Forth and undergoing transition from a terrestrial piedmont-lobe margin with a net surplus of sediment to the south (Dove *et al.*, 2017), to a dynamic, tidewater margin as the ice withdrew into the Firth of Forth (Figure 16).

The combined influence of enhanced flow velocities and grounding line instability triggered by marine inundation of the central North Sea would have been critical mechanisms controlling the development of the mixed-bed signal during deglaciation. Bed excavation in places down to bedrock, increasing bed roughness, till advection and GZW construction were all key feedbacks influencing the landsystem signature. In themselves, the GZWs observed in this study are unusual in that they are not associated with a cross-shelf trough or major fjord system. Instead they chart the retreat of a regional scale, collapsing, marine-based lobate ice stream margin (cf. Patterson, 1997; Jennings, 2006).

Deglaciation: glaciomarine deposition

AF4 was sampled in all the cores in the study area. It is characterised by fine-grained, interlaminated sediments. Micro-scale ripples, and planar cross lamination in some cores indicates underflow activity in a proximal setting close to a grounding line (Figure 9(a); Core 136VC; Smith and Ashley, 1985; Kneller and Buckee, 2000; Mulder and Alexander, 2001). The laminated clays and silts are a product of suspension settling with coarser silt and fine sand laminae representing rain-out from proximal meltwater plumes (Powell, 2003). The frequency of switches in grain size signify an environment dominated by episodic meltwater input. In core 135VC, increasingly distal conditions are marked up-core by a decrease in the frequency of laminae and an increase in the thickness of clay laminae (Figure 8(a)). This is replicated in cores 134VC and 128VC. The abundance of cold water foraminifera species also suggests these are glaciomarine sediments. *Elphidium excavatum (clavatum*) and *Cassidulina reniforme* are known indicators of extreme glacial marine environments, and other indicator species such as *Elphidium incertum, Elphidium asklundi, Elphidium albiumbilicatum, Haynesina orbiculare* and *Bolivina sp.* further corroborate cold glaciomarine conditions (Feyling-Hanssen, 1972; McCabe *et al.*, 1986; Hansen and Knudsen, 1995; Lloyd *et al.*, 2005; Peters *et al.*, 2015)

In cores 132 and 136VC the lower laminated sequences are overlain by diamictic units (Figures 7(b) and 9(a)). This could suggest ice marginal re-advance and the deposition of subglacial till. In 136VC this possibly relates to the margin stabilising on the high ground/pinning points provided by R1-R5 (Figures 3(b), 4(a)). Alternatively, the diamict in 136VC could be a glaciogenic debris flow or mud apron, because two distinctive off-lapping sheets of sediment thicken downslope (north to south) to the basin floor (see core site 136VC in Figures 4(a), (6); cf. Kristensen *et al.*, 2009; Carto and Eyles, 2012; Talling, 2014). Contrary to this, 135VC just to the north of 136VC

shows an increasingly distal record, suggesting it has not been influenced by any local ice marginal re-advances. Core 132VC also contains a diamict sandwiched between two laminated units, indicating a possible later re-advance as ice migrated northward towards M1 and W2. Dropstones in many of the laminated units indicate deposition of ice rafted debris (Thomas and Connell, 1985; Gilbert, 1990; Hart and Roberts, 1994; Ó Cofaigh and Dowdeswell, 2001), although it is noteworthy in 135VC, 136VC and 137VC (Figures 8(a), 9) that the interlaminated facies often lack clasts, possibly inferring sub-ice shelf conditions during retreat (Drewry and Cooper, 1981; Ó Cofaigh and Dowdeswell, 2001), but this requires further investigation.

These sediments have previously been mapped as the Forth, St Abbs and Sunderland Ground Formations across the study area (Figure 2(b); Cameron *et al.*, 1992; Gatliff *et al.*, 1994). From the acoustic data collected as part of this project (Figure 4) they are clearly restricted to small, local basins/depo-centres and as such represent time transgressively deposited pockets of glaciomarine sediment as the NSL receded northwards (Figure 15). A regional signal of increasingly distal conditions is not discernible as each local depo-centre is a repeat package and produced by an active, receding margin (cf. Thomas *et al.*, 2004). AF4 therefore represents a change from proximal to distal conditions through time, and the rhythmicity of the interlaminated sediments is primarily a product of grounding line proximity and changing meltwater flux. The Nye channels mapped north of R12 provide evidence for subglacial meltwater flux to the grounding line, but they are not ubiquitous across the region, hence supraglacial melt could also have been important in influencing water column stratification and mixing (Smith and Ashley, 1985; Cowan and Powell, 1990; Powell, 1990, 2003). AF5 is interpreted as Holocene and contemporary seafloor sediments with gravel lags, poorly sorted sands and shell hash indicative of current reworking across the seafloor (Balson *et al.*, 2001).

Discussion: the Timing and Forcing of Regional Deglaciation

Recent OSL ages from the southern North Sea place the NSL on the Norfolk coast after 22.8–21.5 ka (Roberts *et al.*, 2018). That final phase of NSL advance to the south was followed by ice recession and Dove *et al.* (2017) and Roberts *et al.* (2018) chart a series of large arcuate, lobate moraines formed as the NSL margin migrated north, parallel with the Lincolnshire and Yorkshire coasts (Figure 17). As the ice retreated northwards, Bateman *et al.* (2017) constrain final deglaciation of East Yorkshire coast to >17 ka based on OSL ages relating to the final stages of Glacial Lake Humber at Hemingborough and Ferrybridge and post-glacial sediments found at Barmston and Sewerby (Figure 17). Slightly further north in the Vale of Pickering, Evans *et al.* (2017) suggest the NSL thinned and receded offshore from the Yorkshire coast at ~ 17.6 ka based on ages from Heslerton. Further north again, cosmogenic dates from Tyne Gap show ice had withdrawn westward from the coast by 17.8 to 17.6 ka, although geomorphic evidence indicates that the NSL occupied the coast until slightly later (Livingstone *et al.*, 2015).

The new radiocarbon dates for cores 132VC and 137VC signify deglaciation of the NSL offshore prior to 19.9–19.5 ka cal. BP. These dates are supported by new OSL dates on glacial outwash from Seaham on the Durham coast which suggest final deglaciation after ~ 19.6 ka, as the western margin of the NSL migrated north (Table II). These dates are somewhat earlier (although within errors) than OSL dates from the Yorkshire region (17.6–17 ka; Bateman *et al.*, 2017; Evans *et al.*, 2017) hence further dating control (or recalibration) is required between Lincolnshire, Yorkshire, Durham and Northumberland in order to fully reconcile overall NSL recession rates. However, it is clear from the location of W1 that the NSL had unzipped from the Eden-Stainmore Ice Stream by ~ 19.5 ka, and furthermore, cosmogenic dates west of Newcastle also imply the Tyne gap Ice Stream decoupled from the NSL before ~17.8 ka (Livingstone *et al.*, 2015).

Foraminifera from the distal glaciomarine sediments lying above subglacial till in core 128VC (AF3; Figure 4(a); Table I) signify deglaciation prior to 16.9 ka cal. BP (Figure 17). This age is further supported by onshore dates from the Tay and Forth estuaries where glaciomarine sediments associated with the Errol Beds Formation show ice had moved west of the present coastline by 16.9 to 16.0 ka cal BP (Figure 17; Table III; Hedges *et al.*, 1989; Peacock and Browne, 1998; Peacock, 2002; see Hughes *et al.*, 2011 for overview). An additional Britice-Chrono core (118VC; Figure 17) contains distal glaciomarine sediments lying over subglacial till dated to 17.8 to 16.5 ka cal. BP (Table I), and corroborates the general pattern and rate of ice retreat into the Firth of Forth (though it should be noted that this site lies slightly north of the main flow trajectory of the NSL and, as such, glacier/ice stream dynamics in this region of the Firth of Forth may have been slightly different during deglaciation).

Defining the mechanisms that controlled deglaciation of the NSL between 20 ka and 16 ka is challenging. It is clear from the acoustic stratigraphy and core data that the NSL retreated under glaciomarine conditions. The northern and central NSB was inundated during this period and, although sea-level reconstructions predict that pre-12 ka sea-level was either static (16–20 ka) or falling (16–12 ka) (Bradley *et al.*, 2011), instantaneous inundation would have triggered a grounding line response. The GZW's identified as part of this study (W1 and W2) indicate quasi-stable conditions during overall recession. W1 in particular points to a prolonged period of ice margin stability prior to 17 ka. This is also a period when ice feeding through the Firth of Forth would have experienced significant changes in ice flux, with shifting ice divides over central Scotland. Such changes were a response first to decoupling of the FIS and BIIS (Sejrup *et al.*, 2015; Merritt *et al.*, 2017), followed by air temperature and insolation driven thinning (Alley and Clark, 1999; Bintanja *et al.*, 2005), as well as possible mass balance and dynamic feedbacks relating to westerly sectors of the BIIS responding to the Heinrich 1 cooling (McCabe *et al.*, 1998).

The mixed-bed footprint of the NSL offshore from Durham and Northumberland was therefore a product of several key processes and feedbacks operating during deglaciation, all of which contributed to rapidly changing basal, supraglacial and ice marginal conditions. Marginal instability and drawdown of the NSL were controlled primarily by upstream shifts in ice divide position and regional ice stream flux via the Firth of Forth. Water depths and ice thickness would also have been instrumental in promoting instability at the grounding line. Together with rates of ice surface thinning and meltwater production (increased insolation and air temperatures) these would have been instrumental in lubricating the bed and promoting ice streaming, bed decoupling/basal sliding, bedrock abrasion, till advection, MSGL formation and, ultimately, GZW formation. Hence, in the latter phases of MIS 2 glaciation the NSL was subjected to a complex set of both internal and external driving mechanisms that produced a distinctive mixed-bed subglacial landsystem beneath a retreating, marine-terminating, ice stream lobe in the western North Sea.

Conclusions

New geophysical data, sediment cores and radiocarbon dates from the western North Sea provide fresh insights into the signature and behaviour of the North Sea Lobe during the closing stages of the LGM. Four acoustic facies can be mapped across the study area and interpretations supported using sediments cores. Subglacial tills (AF2 and AF3) form a discontinuous and patchy mosaic of glaciogenic sediments often interspersed with bedrock outcrops and ridges. This mosaic forms a 'mixed-bed' landsystem with bedrock structure and glacial erosion (abrasion and plucking) controlling the position and form of large transverse ridges, but with partial excavation and the net advection of subglacial sediment producing MSGL and GZWs. On a regional scale, this mixed-bed signal of the NSL represents a dynamic switch from a terrestrial streaming piedmont-lobe margin with a net surplus of sediment to the south (Dove *et al.*, 2017), to a partially erosive/excavational, quasi-stable, marine-terminating, ice stream lobe as the ice withdrew northwards.

Glaciomarine sediments are distributed in local depo-centres and basins across the study area and drape the underlying subglacial mixed-bed imprint. The proximal deposition of material was dominated by meltwater plumes, producing thick interlaminated sequences of sands, silts and clays, with secondary inputs from glaciogenic debris flows and underflows. More distal glaciomarine facies are characterised by silts and clays deposited from suspension with additional IRD inputs. Foraminifera assemblages are domainated by *Elphidium clavatum* which is a known indicator of extreme glacial marine environments, and several other species corroborate cold glaciomarine conditions.

In the area offshore from the Durham and Northumberland coasts, new radiocarbon dates suggest that the NSL retreated under tidewater conditions between 19.9 ka and 16.5 ka. This is somewhat earlier than OSL and cosmogenic ages from the Yorkshire coast and Tyne Gap area, but these new ages can be reconciled with deglacial dates from the Tay and Forth estuaries indicative of ice retreat at ~ 16.9 to 16.0 ka cal. BP. The dominant controls on the rates of ice recession and groundling line stability during this period were ice flux through the Firth of Forth ice stream onset zone and water depths at the grounding line, perhaps supplemented by accelerating rates of ice surface thinning and meltwater flux as the climate warmed. However, secondary feedbacks relating to hard to soft bed transition, with bed excavation to partial bedrock, increasing bed roughness, till advection and GZW construction were also key factors influencing the distinctive mixed-bed imprint of a marine-terminating, ice stream lobe in the western North Sea.

Acknowledgements—This work was supported by the EU ITN *Glaciated North Atlantic Margins* (GLANAM) project and Natural Environment Research Council consortium grant*; BRITICE-CHRONO* NE/J009768/1. Data were collected during cruise JC123 in summer 2015. The authors would like to extend their thanks the crew of the RRs James Cook and the BGS and Britice-Chrono science teams who supported the planning and execution of this work. HAS and DD publish with permission of the Executive Director of the British Geological Survey. Multibeam echosounder data shown in Figure 12 were collected as part of the 'Coordination of the Defra Marine Conservation Zone data collection programme 2011/12' funded by the Department of Environment, Food and Rural Affairs of the United Kingdom. The radiocarbon analyses were supported by the NERC Radiocarbon Facility NRCF010001 (allocation number 1976.1015.013). Chris Orton of the Design and Imaging Unit at Durham University is thanked for his help with several figures.

References

Alley R, Clark PU. 1999. The deglaciation of the northern hemisphere: a global perspective. *Annual Review of Earth and Planetary Sciences* **27**: 149–182.

Anderson JB, Bartek LR. 1992. Ross Sea glacial history revealed by high resolution seismic reflection data combined with drill site information. In *The Antarctic Paleoenvironment: A Perspective on Global Change*, Kennett JP, Warnke DE (eds), Vol. **1**, Antarctic Research Series 56. American Geophysical Union: Washington, DC; 231–263.

Balson PS, Jeffrey DH. 1991. The glacial sequence of the southern North Sea. In *Glacial Deposits of Great Britain and Ireland*, Ehlers J, Gibbard PL, Rose J (eds). Balkema: Rotterdam; 245–254.

Balson P, Butcher A, Holmes R, Johnson H, Lewis M, Musson R. 2001. *North Sea Geology*. BGS SEA2 Technical Report.

Batchelor CL, Dowdeswell JA. 2015. Ice-sheet grounding-zone wedges (GZWs) on high-latitude continental margins. *Marine Geology* **363**: 65–92.

Bateman MD, Catt JA. 1996. An absolute chronology for the raised beach deposits at Sewerby, E. Yorkshire, UK. *Journal of Quaternary Science* **11**: 389–395.

Bateman MD, Buckland PC, Chase B, Frederick CD, Gaunt GD. 2008. The Late-Devensian proglacial Lake Humber: new evidence from littoral deposits at Ferrybridge, Yorkshire, England. *Boreas* **37**: 195–210.

Bateman MD, Buckland PC, Whyte MA, Ashurst RA, Boulter C, Panagiotakopulu E. 2011. Re-evaluation of the last glacial maximum typesite at Dimlington, UK. *Boreas* **40**: 573–584.

Bateman MD, Evans DJA, Buckland PC, Connell ER, Friend RJ, Hartmann D, Moxon H, Fairburn WA, Panagiotakopulu E, Ashurst RA. 2015. Last Glacial dynamics of the Vale of York and North Sea Lobes of the British and Irish Ice Sheet. *Proceedings of the Geologist's Association* **126**: 712–730.

Bateman MD, Evans DJA, Roberts DH, Medialdea A, Ely J, Clark CD. 2017. The timing and consequences of the blockage of the Humber Gap by the last British–Irish Ice Sheet. *Boreas* **47**: 41–61.

Bintanja R, van de Wal RS, Oerlemans J. 2005. Modelled atmospheric temperatures and global sea levels over the past million years. *Nature* **437**: 125–128.

Bisat WS. 1932. On the sub-division of the Holderness boulder clays. *The Naturalist Hull*: 215–219.

Booth DB, Hallet B. 1993. Channel networks carved by subglacial water – observations and reconstruction in the eastern Puget Lowland of Washington, USA. *Geological Society of America* **105**: 671–683.

Boston CM, Evans DJA, Ó Cofaigh C. 2010. Styles of till deposition at the margin of the last glacial maximum North Sea lobe of the British–Irish ice sheet: an assessment based on geochemical properties of glacigenic deposits in eastern England. *Quaternary Science Reviews* **29**: 3184–3211.

Boulton GS. 1971. Till genesis and fabric in Svalbard, Spitsbergen. In *Till – A Symposium*, Goldthwait RP (ed). Ohio State University Press: Ohio; 41–72.

Boulton GS. 1975. Processes and patterns of subglacial drainage: a theoretical approach. In *Ice Ages: Ancient and Modern*, Wright AE, Moseley F (eds). Seal House: Liverpool; 7–42.

Boulton GS. 1976. The origin of glacially fluted surfaces: observations and theory. *Journal of Glaciology* **17**: 287–309.

Boulton GS. 1982. Subglacial processes and the development of glacial bedforms. In *Research in Glacial, Glacio-fluvial and Glaciolacustrine Systems*, Davidson-Arnott R, Nickling W, Fahey BD (eds). Geo Books: Norwich; 1–31.

Boulton GS. 1987. A theory of drumlin formation by subglacial sediment deformation. In *Drumlin Symposium*, Menzies J, Rose J (eds). AA Balkema: Rotterdam; 25–80.

Boulton GS. 1996a. The origin of till sequences by subglacial sediment deformation beneath mid-latitude ice sheets. *Annals of Glaciology* **22**: 75–84.

Boulton GS. 1996b. Theory of glacial erosion, transport and deposition as a consequence of subglacial sediment deformation. *Journal of Glaciology* **42**: 43–62.

Boulton GS, Hagdorn M. 2006. Glaciology of the British Isles ice sheet during the last glacial cycle: form, flow, streams and lobes. *Quaternary Science Reviews* **25**: 3359–3390.

Boulton GS, Paul MA. 1976. The influence of genetic processes on some geotechnical properties of tills. *Journal of Engineering Geology* **9**: 159–194.

Boulton GS, Jones AS, Clayton KM, Kenning MJ. 1977. A British ice sheet model and patterns of glacial erosion and deposition in Britain. In *British Quaternary Studies*, Shotton FW (ed). Oxford University Press: Oxford; 231–246.

Boulton GS, Smith GD, Jones AS, Newsome J. 1985. Glacial geology and glaciology of the last mid-latitude ice sheets. *Journal of the Geological Society of London* **142**: 447–474.

Bradley SL, Milne GA, Shennan I, Edwards R. 2011. An improved glacial isostatic adjustment model for the British Isles. *Journal of Quaternary Science* **26**: 541–552.

Bradwell T. 2013. Identifying palaeo-ice-stream tributaries on hard beds: mapping glacial bedforms and erosion zones in NW Scotland. *Geomorphology* **201**: 397–414.

Bradwell T, Stoker MS. 2015. Submarine sediment and landform record of a palaeo-ice stream within the British–Irish Ice Sheet. *Boreas* **44**: 255–276.

Bradwell T, Stoker MS, Larter R. 2007. Geomorphological signature and flow dynamics of The Minch palaeo-ice stream, northwest Scotland. *Journal of Quaternary Science* **22**: 609–617.

Brew DS. 1996. Late Weichselian to early Holocene subaqueous dune formation and burial off the North Sea Northumberland coast. *Marine Geology* **134**: 203–211.

Bronk Ramsey C. 2009. Bayesian analysis of radiocarbon dates. *Radiocarbon* **51**: 337–360.

Cameron TDJ, Crosby A, Balson PS, Jeffrey DH, Lott G, Bulat J, Harrison DJ. 1992. *United Kingdom offshore regional report: the geology of the southern North Sea*. HMSO for the British Geological Survey: London.

Carr SJ, Holmes R, Van Der Meer JJ, Rose J. 2006. The last glacial maximum in the North Sea basin: micromorphological evidence of extensive glaciation. *Journal of Quaternary Science* **21**: 131–153.

Carto SL, Eyles N. 2012. Sedimentology of the Neoproterozoic (*c.* 580 Ma) Squantum 'Tillite', Boston Basin, USA: mass flow deposition in a deep-water arc basin lacking direct glacial influence. *Sedimentary Geology* **269**: 1–14.

Catt JA. 2007. The Pleistocene glaciations of eastern Yorkshire: a review. *Proceedings of the Yorkshire Geological Society* **56**: 177–207.

Clark CD. 1993. Mega-scale glacial lineations and cross-cutting ice-flow landforms. *Earth Surface Processes and Landforms* **18**: 1–29.

Clark CD. 1994. Large-scale ice-moulding: a discussion of genesis and glaciofluvial significance. *Sedimentary Geology* **91**: 253–268.

Clark CD. 2010. Emergent drumlins and their clones: from till dilatancy to flow instabilities. *Journal of Glaciology* **51**: 1011–1025.

Clarke GKC. 2005. Subglacial processes. *Annual Review Earth Planet Science letters* **33**: 247–276.

Clayton L, Atti JW, Mickelson DM. 1999. Tunnel channels formed in Wisconsin during the last glaciation. In *Glacial Processes Past and Present*, Mickelson DM, Attig JW (eds). Geological Society of America, Special Paper **337**, 69–82, Boulder, Colorado.

Colgan PM. 1999. Reconstruction of the Green Bay Lobe, Wisconsin, United States, from 26 000 to 13 000 radiocarbon years. In *Glacial Processes Past and Present*, Mickelson DM, Attig JW (eds). Geological Society of America Special Paper **337**: Boulder, Colorado; 137–150.

Colgan PM, Mickelson DM, Cutler PM. 2003. Ice marginal terrestrial land systems: southern Laurentide ice sheet margin. In *Glacial Land Systems*, Evans DJA (ed). Arnold: London; 111–142.

Cowan EA, Powell RD. 1990. Suspended sediment transport and deposition of cyclically interlaminated sediment in a temperate glacial fjord, Alaska, USA. *Geological Society, London, Special Publications* **53**: 75–89.

Davies BJ, Roberts DH, Ó Cofaigh C, Bridgland DR, Riding J, Philipps ER, Teasdale DA. 2009. Interlobate ice-sheet dynamics during the last glacial maximum at Whitburn Bay, County Durham, England. *Boreas* **38**: 555–578.

Davies BJ, Roberts DH, Bridgland DR, Ó Cofaigh C, Riding JB. 2011. Provenance and depositional environments of Quaternary sediments from the western North Sea basin. *Journal of Quaternary Science* **26**: 59–75.

Davies BJ, Roberts DH, Bridgland DR, Ó Cofaigh C. 2012a. Dynamic Devensian ice flow in NE England: a sedimentological reconstruction. *Boreas* **41**: 337–336.

Davies BJ, Roberts DH, Bridgland DR, Ó Cofaigh C, Riding JB, Demarchi B, Penkman KEH, Pawley SM. 2012b. Timing and depositional environments of a Middle Pleistocene glaciation of northeast England: new evidence from Warren House Gill, County Durham. *Quaternary Science Reviews* **44**: 180–212.

Dove D, Arosio R, Finlayson A, Bradwell T, Howe JA. 2015. Submarine glacial landforms record Late Pleistocene ice-sheet dynamics, Inner Hebrides, Scotland. *Quaternary Science Reviews* **123**: 76–90.

Dove D, Evans DJA, Lee JR, Roberts DH, Tappin DR, Mellett CL, Long D, Callard SL. 2017. Phased occupation and retreat of the last British–Irish Ice Sheet in the southern North sea; geomorphic and seismostratigraphic evidence of a dynamic ice lobe. *Quaternary Science Reviews* **163**: 114–134.

Dowdeswell JA, Ó Cofaigh C, Pudsey CJ. 2004. Thickness and extent of the subglacial till layer beneath an Antarctic paleo–ice stream. *Geology* **32**: 13–16.

Dredge LA, Cowan WR. 1989. Quaternary geology of the southwestern Canadian Shield. In *Quaternary Geology of Canada and Greenland*, Fulton RT (ed). Geological Survey of Canada, Ottawa: Geology of Canada, 1: 214–235.

Drewry DJ, Cooper APR. 1981. Processes and models of Antarctic glaciomarine sedimentation. *Annals of Glaciology* **2**: 117–122.

Ely JC, Clark CD, Spagnolo M, Hughes ALC, Stokes CR. 2018. Using the size and position of drumlins to understand how they grow, interact and evolve. *Earth Surface Processes and Landforms* **43**: 1073–1087.

Evans DJA, Benn D. 2004. *A Practical Guide to the Study of Glacial Sediments*. Arnold: London.

Evans DJA, Hiemstra JF. 2005. Till deposition by glacier submarginal, incremental thickening. *Earth Surface Processes and Landforms* **30**: 1633–1662.

Evans DJA, Thomson SA. 2010. Glacial sediments and landforms of Holderness, eastern England: a glacial depositional model for the North Sea Lobe of the British–Irish Ice Sheet. *Earth Science Reviews* **101**: 147–189.

Evans DJA, Owen LA, Roberts DH. 1995. Stratigraphy and sedimentology of Devensian (Dimlington-Stadial) glacial deposits, East Yorkshire, England. *Journal of Quaternary Science* **10**: 241–265.

Evans DJA, Clark CD, Mitchell WA. 2005. The last British Ice Sheet: a review of the evidence utilised in the compilation of the Glacial Map of Britain. *Earth-Science Reviews* **70**: 253–312.

Evans DJA, Clark CD, Rea BR. 2008. Landform and sediment imprints of fast glacier flow in the southwest Laurentide Ice Sheet. *Journal of Quaternary Science* **23**: 249–272.

Evans DJA, Hiemstra JF, Boston C, Leighton I, Ó Cofaigh C, Rea BR. 2012. Till stratigraphy and sedimentology at the margins of terrestrially terminating ice streams: case study of the western Canadian prairies and high plains. *Quaternary Science Reviews* **46**: 80–125.

Evans DJA, Young NJP, Ó Cofaigh C. 2014. Glacial geomorphology of terrestrial-terminating fast flow lobes/ice stream margins in the southwest Laurentide Ice Sheet. *Geomorphology* **204**: 86–113.

Evans DJA, Bateman MD, Roberts DH, Medialdea A, Hayes L, Duller GAT, Fabel D, Clark CD. 2017. Glacial Lake Pickering: stratigraphy and chronology of a proglacial lake dammed by the North Sea Lobe of the British–Irish Ice Sheet. *Journal of Quaternary Science* **32**: 295–310.

Everest J, Bradwell T, Golledge N. 2005. Subglacial landforms of the Tweed Palaeo-Ice stream. *The Scottish Geographical Magazine* **121**: 163–173.

Eyles N, Doughty M. 2016. Glacially-streamlined hard and soft beds of the paleo-Ontario ice stream in Southern Ontario and New York state. *Sedimentary Geology* **338**: 51–71.

Eyles N, Sladen JA, Gilroy S. 1982. A depositional model for stratigraphic complexes and facies superimposition in lodgement tills. *Boreas* **11**: 317–333.

Eyles N, McCabe AM, Bowen DQ. 1994. The stratigraphic and sedimentological significance of Late Devensian ice sheet surging in Holderness, Yorkshire, UK. *Quaternary Science Reviews* **13**: 727–759.

Eyles N, Putkinen N, Sookhan S, Arbelaez-Moreno L. 2016. Erosional origin of drumlins and megaridges. *Sedimentary Geology* **338**: 2–23.

Fannin NGT. 1989. *Offshore Investigations 1966–1987*. British Geological Survey Technical Report WB/89/2.

Feyling-Hanssen RW. 1972. The foraminifer Elphidium excavatum (Terquem) and its variant forms. *Micropaleontology* **18**: 337–354.

Gatliff R, Richards P, Smith K, Graham CC, McCormac M, Smith NJP, Long D, Cameron TD, Evans D, Stevenson AG, Bulat J, Ritchie JD. 1994. *United Kingdom offshore regional report: the geology of the central North Sea*. HMSO for the British Geological Survey: London.

Gilbert R. 1990. Rafting in glacimarine environments. In *Glacimarine Environments: Processes and Sediments*, Dowdeswell JA, Scourse JD (eds). Geological Society Special Publication, London, **53**: 105–120.

Golledge NR, Stoker MS. 2006. A palaeo-ice stream of the British Ice Sheet in eastern Scotland. *Boreas* **35**: 231–243.

Graham AGC, Lonergan L, Stoker MS. 2007. Evidence for Late Pleistocene ice stream activity in the Witch Ground Basin, central North Sea, from 3D seismic reflection data. *Quaternary Science Reviews* **26**: 627–643.

Graham AGC, Stoker MS, Lonergan L, Bradwell T, Stewart MA. 2011. The Pleistocene glaciations of the North Sea basin. In *Developments in Quaternary Science: Quaternary Glaciations – Extent and Chronology: a Closer Look*, Ehlers J, Gibbard PL, Hughes PD (eds). Elsevier: Amsterdam; 261–268.

Gravenor CP, Von Brunn V, Dreimanis A. 1984. Nature and classification of waterlain glaciogenic sediments, exemplified by Pleistocene, Late Paleozoic and Late Precambrian deposits. *Earth-Science Reviews* **20**: 105–166.

Hansen A, Knudsen KL. 1995. Recent foraminiferal distribution in Freemansundet and Early Holocene stratigraphy on Edgeøya, Svalbard. *Polar Research* **14**: 215–238.

Harkness DD, Wilson HW. 1979. Scottish universities research and reactor centre radiocarbon measurements III. *Radiocarbon* **21**: 203–256.

Hart JK, Roberts DH. 1994. Criteria to distinguish between subglacial glaciotectonicand glaciomarine sedimentation, I. Deformation styles and sedimentology. *Sedimentary Geology* **91**: 1–382.

Hedges REM, Housle RA, Law IA, Bronk CR. 1989. Radiocarbon dates from the Oxford AMS system: archaeometry datelist 9. *Archaeometry* **31**: 207–234.

Hogan KA, Ó Cofaigh C, Jennings AE, Dowdeswell JA, Hiemstra JF. 2016. Deglaciation of a major palaeo-ice stream in Disko Trough, West Greenland. *Quaternary Science Reviews* **147**: 5–26.

Hubbard AL, Bradwell T, Golledge N, Hall A, Patton H, Sugden D, Cooper R, Stoker MS. 2009. Dynamic cycles, ice streams and their impact on the extent, chronology and deglaciation of the British–Irish ice sheet. *Quaternary Science Reviews* **28**: 758–776.

Hughes ALC, Greenwood SL, Clark CD. 2011. Dating constraints on the last British–Irish Ice Sheet: a map and database. *Journal of Maps* **7**: 156–184.

Hutton K. 2018. The glacial geomorphology of the Firth of Forth. Unpublished MRes thesis, University of Durham.

Huuse M, Lykke-Anderson H. 2000. Over-deepened Quaternary valleys in the eastern Danish North sea: morphology and origin. *Quaternary Science Reviews* **19**: 1233–1253.

Iverson NR. 2010. Shear resistance and continuity of till at glacier beds: hydrology rules. *Journal of Glaciology* **56**: 1104–1114.

Iverson NR, Jansson P, Hooke RL. 1994. *In situ* measurements of the strength of deforming subglacial till. *Journal of Glaciology* **40**: 497–503.

Jansson KN, Kleman J. 1999. The horned crag-and-tails of the Ungava Bay landform swarm, Québec-Labrador, Canada. *Annals of Glaciology* **28**: 168–174.

Jennings CE. 2006. Terrestrial ice streams: a view from the lobe. *Geomorphology* **75**: 100–124.

Jennings AE, Walton ME, Ó Cofaigh C, Kilfeather A, Andrews JT, Ortiz JD, De Vernal A, Dowdeswell JA. 2014. Paleoenvironments during Younger Dryas–Early Holocene retreat of the Greenland Ice Sheet from outer Disko Trough, central west Greenland. *Journal of Quaternary Science* **29**: 27–40.

Kilfeather AA, Ó Cofaigh C, Lloyd JM, Dowdeswell JA, Xu S, Moreton SG. 2011. Ice-stream retreat and ice-shelf history in Marguerite Trough, Antarctic Peninsula: sedimentological and foraminiferal signatures. *Geological Society of America Bulletin* **123**: 997–1015.

Kneller B, Buckee C. 2000. The structure and fluid mechanics of turbidity currents: a review of some recent studies and their geological implications. *Sedimentology* **47**: 62–94.

Kovanen DJ, Slaymaker O. 2004. Glacial imprints of the Okanogan Lobe, southern margin of the Cordilleran Ice Sheet. *Journal of Quaternary Science* **19**: 547–565.

Krabbendam M, Eyles N, Putkinen N, Bradwell T, Arbelaez-Moreno L. 2016. Streamlined hard beds formed by palaeo-ice streams: a review. *Sedimentary Geology* **338**: 24–50.

Kristensen L, Benn DI, Hormes A, Ottesen D. 2009. Mud aprons in front of Svalbard surge moraines: evidence of subglacial deforming layers or proglacial glaciotectonics? *Geomorphology* **111**: 206–221.

Lamplugh GW. 1879. On the divisions of the glacial beds in Filey Bay. *Proceedings of the Yorkshire Geological and Polytechnic Society* **1**: 161–177.

Livingstone SJ, Evans DJA, Ó Cofaigh C, Davies BJ, Merritt JW, Huddart D, Mitchell WA, Roberts DH, Yorke L. 2012. Glaciodynamics of the central sector of the last British–Irish Ice Sheet in Northern England. *Earth Science Reviews* **111**: 25–55.

Livingstone SJ, Roberts DH, Davies BJ, Evans DJA, Ó Cofaigh C, Gheorghiu DM. 2015. Late Devensian deglaciation of the Tyne Gap Palaeo-Ice stream, northern England. *Journal of Quaternary Science* **30**: 790–804.

Lloyd JM, Park LA, Kuijpers A, Moros M. 2005. Early Holocene palaeoceanography and deglacial chronology of Disko Bugt, West Greenland. *Quaternary Science Reviews* **24**: 1741–1755.

McCabe AM, Haynes JR, Macmillan NF. 1986. Late-Pleistocene tidewater glaciers and glaciomarine sequences from north County Mayo, Republic of Ireland. *Journal of Quaternary Science* **1**: 73–84.

McCabe AM, Knight J, McCarron S. 1998. Evidence for Heinrich Event 1 in the British Isles. *Journal of Quaternary Science* **13**: 549–568.

Merritt JW, Connell RE, Hall AM. 2017. Middle to Late Devensian glaciation of north-east Scotland: implications for the north-eastern quadrant of the last British–Irish ice sheet. *Journal of Quaternary Science* **32**: 276–294.

Mulder T, Alexander J. 2001. The physical character of subaqueous sedimentary density flows and their deposits. *Sedimentology* **48**: 269–299.

Murray AS, Wintle AG. 2003. The single aliquot regenerative dose protocol: potential for improvements in reliability. *Radiation Measurements* **37**: 377–381.

Ó Cofaigh C. 1996. Tunnel valley genesis. *Progress in Physical Geography: Earth and Environment* **20**: 1–19.

Ó Cofaigh C, Dowdeswell JA. 2001. Laminated sediments in glacimarine environments: diagnostic criteria for their interpretation. *Quaternary Science Reviews* **20**: 1411–1436.

Ó Cofaigh C, Dowdeswell JA, Allen CS, Hiemstra JF, Pudsey CJ, Evans J, Evans DJ. 2005. Flow dynamics and till genesis associated with a marine-based Antarctic palaeo-ice stream. *Quaternary Science Reviews* **24**: 709–740.

Ottesen D, Dowdeswell JA. 2006. Assemblages of submarine landforms produced by tidewater glaciers in Svalbard. *Journal of Geophysical Research: Earth Surface* **111**: F01016. https://doi.org/10.1029/2005JF000330.

Ottesen D, Dowdeswell JA, Lanvik JY, Mienert J. 2007. Dynamics of the Late Weichselian ice sheet on Svalbard inferred from high-resolution sea-floor morphology. *Boreas* **36**: 286–306.

Ottesen D, Stokes CR, Bøe R, Rise L, Longva O, Thorsnes T, Olesen O, Bugge T, Lepland A, Hestvik OB. 2016. Landform assemblages and sedimentary processes along the Norwegian Channel Ice Stream. *Sedimentary Geology* **338**: 115–137.

Patterson CJ. 1997. Southern Laurentide ice lobes were created by ice streams: Des Moines Lobe in Minnesota, USA. *Sedimentary Geology* **111**: 249–261.

Patterson CJ. 1998. Laurentide glacial landscapes: the role of ice streams. *Geology* **26**: 643–646.

Patton H, Hubbard AL, Andreassen K, Auriac A, Whitehouse PL, Stroeven AP, Shackleton C, Winsborrow MCM, Heyman J, Hall AM. 2017. Deglaciation of the Eurasian ice sheet complex. *Quaternary Science Reviews* **169**: 148–172.

Peacock JD. 1999. The Pre-Windermere Interstadial (Late Devensian) raised marine strata of eastern Scotland and their macro- fauna: a review. *Quaternary Science Reviews* **18**: 1655–1680.

Peacock JD. 2002. Macrofauna and palaeoenvironment of marine strata of Windermere Interstadial age on the east coast of Scotland. *Scottish Journal of Geology* **38**: 31–40.

Peacock JD, Browne MAE. 1998. Radiocarbon dates from the Errol Beds (pre-Windermere Interstadial raised marine deposits) in eastern Scotland. *Quaternary Newsletter* **86**: 1–7.

Peters JL, Benetti S, Dunlop P, Ó Cofaigh C. 2015. Maximum extent and dynamic behaviour of the last British–Irish Ice Sheet west of Ireland. *Quaternary Science Reviews* **128**: 48–68.

Powell RD. 1990. Glaciomarine processes at grounding line fans and their growth to ice contact deltas. In *Glaciomarine Environments: Processes and Sediments*, Dowdeswell JA, Scourse JD (eds). Geological Society Special Publication, London, **52**; 53–73.

Powell RD. 2003. Subaquatic landsystems: Fjords. In *Glacial Landsystems*, Evans DJA (ed). Arnold: London; 313–347.

Powell RD, Alley RB. 1997. Grounding-line systems: processes, glaciological inferences and the stratigraphic record. In *Geology and Seismic Stratigraphy of the Antarctic Margin*, Barker PF, Cooper AK (eds). Antarctic Research Series **2**: 169–187. Geological Society, London.

Powell RD, Domack EW. 1995. Modern glaciomarine environments. In *Glacial Environments: Volume 1. Modern Glacial Environments: Processes, Dynamics and Sediments*, Menzies J (ed). Butterworth-Heinmann: Oxford; 445–486.

Praeg D. 2003. Seismic imaging of mid-Pleistocene tunnel-valleys in the North Sea Basin – high resolution from low frequencies. *Journal Applied Geophysics* **53**: 273–298.

Prescott JR, Hutton JT. 1994. Cosmic ray contributions to dose rates for luminescence and ESR: large depths and long-term time variations. *Radiation Measurements* **23**: 497–500.

Reimer P, Bard E, Bayliss A, Beck J, Blackwell P, Ramsey C, Van der Plicht J. 2013. IntCal13 and Marine13 Radiocarbon Age Calibration Curves 0–50,000 Years cal BP. *Radiocarbon* **55**: 1869–1887.

Roberts DH, Evans DJA, Lodwick J, Cox NJ. 2013. The subglacial and icemarginal signature of the North Sea lobe of the British Irish Ice Sheet during the last glacial maximum at Upgang, North Yorkshire, UK. *Proceedings of the Geologists' Association* **124**: 503–519.

Roberts DH, Evans DJA, Callard SL, Dove D, Bateman MD, Medialdea A, Saher M, Ó Cofaigh C, Chiverrell RC, Moreton SG, Cotterill CJ, Clark CD. 2018. The MIS II limit of the British-Irish Ice Sheet in the Southern North sea. *Quaternary Science Reviews* **198**: 181–207.

Schoof C. 2007. Ice sheet grounding line dynamics: steady states, stability, and hysteresis. *Journal of Geophysical Research* **112**: F03S28. https://doi.org/10.1029/2006JF000664.

Sejrup HP, Hjelstuen BO, Nygard A, Haflidason H, Mardal I. 2015. Late Devensian ice-marginal features in the central North sea – processes and chronology. *Boreas* **44**: 1–13.

Sejrup HP, Clark CD, Hjelstuen BO. 2016. Rapid ice sheet retreat triggered by ice stream de-buttressing: evidence from the North Sea. *Geology* **44**: 355–358.

Shreve RL. 1972. Movement of water in glaciers. *Journal of Glaciology* **11**: 205–214.

Slota PJ, Jull AJ, Linick TW, Toolin LJ. 1987. Preparation of small samples for 14 C accelerator targets by catalytic reduction of CO. *Radiocarbon* **29**: 303–306.

Smith ND, Ashley GM. 1985. Proglacial lacustrine environment, physical processes. In *Glacial Sedimentary Environments*, Ashley GM, Shaw J, Smith ND (eds), Vol. **16**. Society of Economic Paleontologists and Mineralogists, Short Course No; 135–217.

Spagnolo M, Clark CD, Ely JC, Stokes CR, Anderson JB, Andreassen K, Graham AGC, Kin EC. 2014. Size, shape and spatial arrangement of mega-scale glacial lineations from a large and diverse dataset. *Earth Surface Processes and Landforms* **39**: 1432–1448.

Stoker MS, Bent A. 1985. Middle Pleistocene glacial and glaciomarine sedimentation in the west central North sea. *Boreas* **14**: 325–332.

Stokes CR, Clark CD. 2001. Palaeo-ice streams. *Quaternary Science Reviews* **20**: 1437–1457.

Stokes CR, Clark CD. 2002. Are long subglacial bedforms indicative of fast ice flow? *Boreas* **31**: 239–249.

Stokes CR, Fowler AC, Clark CD, Hindmarsh RCA, Spagnolo M. 2013. The instability theory of drumlin formation and its explanation of their varied composition and internal structure. *Quaternary Science Reviews* **62**: 77–96.

Talling PJ. 2014. On the triggers, resulting flow types and frequencies of subaqueous sediment density flows in different settings. *Marine Geology* **352**: 155–182.

Teasdale D. 2013. Evidence for the western limits of the North Sea Lobe of the BIIS in North East England. In *The Quaternary of Northumberland, Durham and Yorkshire Field Guide*, Davies BJ, Yorke L, Bridgland DR, Roberts DH (eds). Quaternary Research Association: London; 106–121.

Thomas GSP, Connell RJ. 1985. Iceberg drop, dump, and grounding structures from Pleistocene glacio-lacustrine sediments, Scotland. *Journal of Sedimentary Research* **55**: 243–249.

Thomas GSP, Chiverrell RC, Huddart D. 2004. Ice-marginal depositional responses to probable Heinrich events in the Devensian deglaciation of the Isle of Man. *Quaternary Science Reviews* **23**: 85–106.

Thomsen KJ, Murray AS, Bøtter-Jensen L, Kinahan J. 2007. Determination of burial dose in incompletely bleached fluvial samples using single grains of quartz. *Radiation Measurements* **42**: 370–379.

Wood SV, Rome JL. 1868. On the glacial and postglacial structure of Lincolnshire and south-east Yorkshire. *Quarterly Journal of the Geological Society* **24**: 2–3.

Supporting Information

Additional supporting information may be found online in the Supporting Information section at the end of the article.

Data S1. Supporting information

Data S2. Supporting information

Data S3. Supporting information

Data S4. Supporting information

Data S5. Supporting information

Data S6. Supporting information

Data S7. Supporting information

Data S8. Supporting information